INVESTIGATION OF PROTEIN ADSORPTION AND CELL BEHAVIOR ON LASER-TEXTURED TITANIUM SURFACES

by

Şeyma Soykan

B.S., in Biomedical Engineering, Yeditepe University, 2021

Submitted to the Institute of Biomedical Engineering
in partial fulfillment of the requirements
for the degree of
Master of Science
in
Biomedical Engineering

Boğaziçi University
2024

INVESTIGATION OF PROTEIN ADSORPTION AND CELL BEHAVIOR ON LASER-TEXTURED TITANIUM SURFACES

APPROVED BY:

Prof. Dr. Bora Garipcan ..... (Thesis Advisor)

Assistant Prof. Dr. Hasret Tolga Şirin .....

Assistant Prof. Dr. Mustafa Kemal Ruhi .....

DATE OF APPROVAL: 16 August 2024

ACKNOWLEDGMENTS

First of all, I would like to express my appreciation to my thesis advisors Dr. Bora Garipcan and Dr. Ebru Akdoğan for their outspoken support and guidance. I appreciate the attendance and enjoyable contribution of Dr. Hasret Tolga Şirin to our remote meetings. I feel very lucky to gain my first research experiences under their mentorship.I would like to thank Dr. Seydi Yavaş and his team for their harmonious collaboration and sharing their facilities. I would like to thank my mom, dad and sweet sisters for always being with my side. Life would be harder without their existence. I want to thank my dearest colleagues and friends in Biomimetic and Bioinspired Biomaterials Laboratory Group. Specially, Berkay, Fatma and Hayriye for never declining my questions and for all their support in every possible way to help me. Additionally, i want to express my happiness to have Ebru Saraç in my life. I'm glad to grow as we go. All of my friends i had during my master journey are as valuable as experiences i got during these three years. Between all these academic struggles, i always feel grateful for the existence of my horse-riding teammate Emine, our coach and my sweet girl Queen.

This thesis was financially and morally supported by Dr. Garipcan and Dr. Akdoğan.

I am dedicating this thesis to my 23 years old-self who believes everything could be figured out by working. Working is a bigger portion of solving things, but everything has its own time to be totally fulfilled. Thus, do not be in hurry, try to enjoy the process and do not let the reality lose your passion for whatever you do.

ACADEMIC ETHICS AND INTEGRITY STATEMENT

I, Şeyma Soykan, hereby certify that I am aware of the Academic Ethics and Integrity Policy issued by the Council of Higher Education (YÖK) and I fully acknowledged all the consequences due to its violation by plagiarism or any other way.

Name :

Signature:

Date:

ABSTRACT

INVESTIGATION OF PROTEIN ADSORPTION AND CELL BEHAVIOR ON LASER-TEXTURED TITANIUM SURFACES

When an implant introduced to the body, proteins in the blood stream cover the implant surface. That is how the body starts to recognizes foreign materials. The properties of surface plays critical role to predict the body response by understanding protein adsorption. Surface texturing using lasers is an effective and highly controllable surface modification technique. This thesis is focused on distinct surface patterns formed by microsecond and femtosecond lasers to observe the protein adsorption and cell behavior on titanium (Ti) surfaces. Ti has been chosen as the model biomaterial since it is a widely used material as a bone implant which mimics the bone structure in terms of strength and density. We hypothesized that periodic nano-morphology on Ti surfaces obtained using different laser sources will affect the protein adsorption, cell attachment and proliferation. The study has 4 aspects; surface modification, surface characterization, protein and cell culture studies. Surfaces had 3 patterns; polished (pTi), laser textured by microsecond laser (mTi) and by femtosecond laser (fTi).Surfaces were characterized in terms of wettability, roughness and topography. Protein amount and conformational changes of proteins were investigated. Adsorbed protein amount was higher on pTi compared to the other groups. Cytotoxicity and cell proliferation were examined. While cytotoxicity was not observed in results of indirect MTT assay, Ti samples showed cytotoxic effect in the results of direct MTT assay. fTi demonstrated significantly high proliferation rate compared to mTi and pTi. Cell morphology and alignment was investigated. As a result of this thesis, forming submicron patterns based on laser texturing significantly influences the protein adsorption, protein conformation, cell proliferation and cell morphology.

Keywords: Protein adsorption, Titanium, Nano-morphology, Femtosecond Laser, Cell-Biomaterial Interactions.

ÖZET

Lazerle Desenlenmiş Titanyum Yüzeylerinde Hücre Davranışının ve Protein Adsorpsiyonunun İncelenmesi

Vücuda bir implant yerleştirildiğinde, ilk olarak proteinler implantın yüzeyine yapışarak bir protein katmanı oluşturur. Vücudun biyomalzemeyi tanımaya başlaması bu protein katmanının özellikleriyle bağlantılıdır. Biyomalzeme yüzey özellikleri protein adsorpsiyonunu anlayarak vücudun tepkisini tahmin etmek açısından kritik bir rol oynar. Yüzeylerin lazerle işlenmesi, son derece kontrol edilebilir bir yöntem olduğu için etkili bir modifikasyon tekniğidir. Bu tezin odağı, mikrosaniye ve femtosaniye lazerlerle işlenmiş birbirinden farklı periyodik yüzey desenlerine sahip titanyumlarda protein adsorpsiyon ve hücre davranışının araştırılmasıdır. Titanyum (Ti), kemiğin yapısını güç ve yoğunluk açısından taklit edebilen bir kemik implantı olduğu için model biyomalzeme olarak seçilmiştir. Hipotezimiz, farklı lazer kaynaklarıyla elde edilen periyodik nano-morfolojinin protein adsorpsiyonu ve hücre çoğalması üzerinde etkisi olacağı yönündedir. Bu amaçla çalışma 4 aşamaya bölünmüştür; biyomalzeme yüzey modifikasyonu, yüzey karakterizasyonu, protein ve hücre çalışmaları. Yüzeyler 3 farklı desene sahiptir; parlatılmış (pTi), mikro saniye lazerle (mTi) ve femtosaniye lazerle (fTi) işlenmiş. Yüzeyler,ıslatabilirlik, yüzey topografisi ve pürüzlülük açısından karakterize edilmiştir. Protein adsorpsiyon miktarı ve konformasyonel değişiklikler incelenmiştir. En yüksek protein tutunması, pTi grubunda gözlemlenmiştir. Sitotoksisite ve hücre proliferasyonu incelenmiştir. Sonuçlara göre indirekt MTT analizinde toksik etki gözlemlenmezken, direkt MTT analizinde toksik etkiye rastlanmıştır. fTi grubu daha yüksek bir hücre proliferasyonu göstermiştir. Hücre morfolojisi ve dağılımı incelenmiştir. Bu tezin sonucunda, lazerle işlenen nano boyutlu desenlerin protein adsorpsiyonunda, konformasyonel değişikliklerde ve hücre davranışında etkisi olduğu gözlemlenmiştir.

Anahtar Sözcükler: Protein Adsorpsiyonu, Nanomorfoloji, Femtosaniye Lazer, Hücre-Biyomalzeme Etkileşimi

TABLE OF CONTENTS

ACKNOWLEDGMENTS . . . iii
ACADEMIC ETHICS AND INTEGRITY STATEMENT . . . iv
ABSTRACT . . . v
ÖZET . . . vi
LIST OF FIGURES . . . x
LIST OF TABLES . . . xii
LIST OF SYMBOLS . . . xiii
LIST OF ABBREVIATIONS . . . xiv
1. INTRODUCTION . . . 1
1.1 Motivation . . . 1
1.2 Objective . . . 3
1.3 Outline . . . 4
2. BACKGROUND . . . 5
2.1 Bone Structure . . . 5
2.2 Bone Cells . . . 5
2.3 Biomaterials . . . 7
2.4 Biomaterials Used for Bone Tissue . . . 7
2.5 Titanium . . . 9
2.6 Biomaterial-Tissue Interface . . . 9
2.7 Surface Modification . . . 10
2.8 Protein Adsorption . . . 10
2.9 Cell-Biomaterial Interactions . . . 13
2.10 LASER . . . 13
2.11 Laser Surface Modifications . . . 14
3. MATERIALS AND METHODS . . . 16
3.1 Preparation of Titanium Samples . . . 17
3.2 Surface Modifications of Titanium Samples . . . 17
3.3 Surface Characterization of Ti Samples . . . 18
3.3.1 Surface Topography . . . 18

3.3.2 Surface Wettability 18
3.3.3 Surface Roughness 18
3.4 Protein Adsorption Analysis 19
3.4.1 X-Ray Photoelectron Spectroscopy (XPS) 19
3.4.2 Fourier Transform Infrared Spectroscopy (FTIR) 19
3.5 Cell Culture Studies 20
3.5.1 Sample Preparation for Cell Culture Studies 20
3.5.2 MTT Cell Cytotoxicity Assay 20
3.5.3 Indirect MTT Cytotoxicity Assay 21
3.5.4 Direct MTT Cytotoxicity Assay 21
3.5.5 alamarblue Cell Proliferation Assay 22
3.5.6 Evaluation of Cell Morphology 22
3.5.7 Scanning Electron Microscopy (SEM) Imaging 22
3.5.8 Fluorescent Imaging 22
4. RESULTS 24
4.1 Material Characterization 24
4.1.1 Investigation of Ti Surface Patterns 24
4.1.2 Water Contact Angle Measurement (WCA) 25
4.1.3 Atomic Force Microscopy Measurements (AFM) 26
4.2 Protein Studies 28
4.2.1 X-Ray Photo-electron Spectroscopy (XPS) 28
4.2.2 Fourier Transform Infrared Spectroscopy (FTIR) 30
4.3 CELL CULTURE STUDIES 32
4.3.1 Indirect MTT Cytotoxicity Assay 32
4.3.2 Direct MTT Cytotoxicity Assay 32
4.3.3 alamarBlue Cell Proliferation Assay 33
4.3.4 Morphology of MC3TC3-E1 Cells 34
4.3.5 Fluorescent Staining 35
4.4 Statistical Analysis 36
5. DISCUSSION 37
5.1 Material Characterization 37
5.2 Protein Adsorption Studies 39

5.3 Cell Culture Studies 40
6. CONCLUSION 42
6.1 Further Studies 42
REFERENCES 44

LIST OF FIGURES

Figure 2.1	Illustration of bone cells draw by using Canva.	7
Figure 2.2	Summary of parameters affecting the protein adsorption mechanism draw by using Canva.	12
Figure 2.3	Illustration of long pulsed (a) and short pulsed laser (b) effect on surface. SEM images of laser ablated holes (c. nanosecond laser, d. femtosecond laser) on steel coil [1]	15
Figure 3.1	Schematic representation of modified Ti surfaces. A) pTi, B) mTi, C) fTi.	17
Figure 4.1	SEM images of Ti samples. A) pTi, B) mTi, C) fTi. Scale bars from left to right; 50 μm, 20 μm, 10 μm and 5 μm.	25
Figure 4.2	Water contact angle measurements of pTi, mTi and fTi surfaces. B) Images of water droplets from top to down is; pTi, mTi and fTi. Error bars representing the standard deviation.	25
Figure 4.3	Roughness parameters of I) pTi, II) mTi and III) fTi samples. A) AFM images were taken in area of 50 μm x 50 μm. Scale bars show 5 μm distance. B) 3D profiles of the samples. C) Line profiles of titanium samples. D) Height distribution graphs of the samples.	27
Figure 4.4	XPS Analysis of protein adsorption on Ti samples. A) Survey spectra of Ti surfaces. Teal colored line is demonstrating peaks following to the protein adsorption while pink colored line showing the peaks prior to the protein adsorption. B) Ti_{2p} high resolution spectra of pTi, mTi and fTi surfaces upon protein adsorption. C) N_{1s} high resolution spectra of pTi, mTi and fTi surfaces upon protein adsorption.	29
Figure 4.5	amide-I band of BSA at 1645 cm^{-1} on A) pTi, 1651 cm^{-1} on B) mTi and 1645 cm^{-1} on C) fTi samples with deconvoluted peaks of secondary structure components	31

Figure 4.6 A) Results of Indirect MTT cytotoxicity assay of L929 fibroblast cells on pTi, mTi, fTi, PC and NC surfaces. (PC: positive control, NC: negative control) B) Results of Direct MTT cytotoxicity assay of L929 fibroblast cells on pTi, mTi, fTi and TCPS. (TCPS: Positive control.) (**:p<0.01) (****:p<0.0001) 32

Figure 4.7 alamarBlue cell proliferation assay to assess the effect of MC3T3-E1 proliferation on the pTi, mTi and fTi surfaces. (*: p<0.05, ****: p<0.0001) (TCPS: positive control) 33

Figure 4.8 SEM images of MC3T3-E1 pre-osteoblast cells on I) pTi, II) mTi, III) fTi samples. Cells were imaged with a. 100X b.500X c.1000X d.2000X e.5000X f.10000X g.20000X magnifications. In the same order, scales bars are demonstrating 500 μm, 100 μm, 50 μm, 20 μm, 10 μm, 5 μm and 2 μm distance. 34

Figure 4.9 Nuclear (DAPI) and actin skeleton (Phalloidin) staining of MC3T3-E1 cells on Ti samples. A) TCPS:positive control, B) pTi, C) fTi, D) mTi. The surface patterns are shown on the upper inlet SEM photos of corresponding Ti samples. 35

LIST OF TABLES

Table 3.1	Deconvoluted amide-I band frequencies and assigned protein secondary structure components.Data are from [2], [3].	20
Table 4.1	The roughness values of Ti sample surfaces calculated from AFM analysis.	26
Table 4.2	Peak Positions and Atomic Ratios of Elements on the BSA-adsorbed Ti Samples	28
Table 4.3	Wavenumbers of BSA secondary structure upon adsorption on pTi, mTi and fTi surfaces. (NA: Not announced. "- ": not exist in native BSA structure	30
Table 4.4	Percent Area of BSA secondary structure upon adsorption on pTi, mTi and fTi surfaces. (NA: Not announced. "- ": not exist in native BSA structure	30

LIST OF SYMBOLS

Ar	Argon
GPa	Gigapascal
g/L	Gram per liter
μL	Microliter
μm	Micrometer
nm	Nanometer
%	Percentage

LIST OF ABBREVIATIONS

AFM	Atomic Force Microscopy
ATCC	American Type Culture Collection
BLC	Bone Lining Cells
Co-Cr	Cobalt Chromium
DMSO	Dimethyl Sulfoxide
ECM	Extracellular Matrix
fs laser	Femtosecond Laser
fTi	Femtosecond Laser Textured Titanium
FBR	Foreign Body Response
FTIR	Fourier-Transform Infrared Spectroscopy
LIPSS	Laser Induced Periodic Surface Structures
μs laser	Microsecond Laser
mTi	Microsecond Laser textured titanium
pTi	Polished titanium
PEG	Polyethylene Glycol
PCL	Polycaprolactone
PGA	Polyglycolic acid
PLA	Polylactic acid
SEM	Scanning Electron Microscopy
Ti	Titanium
TCP	Tricalcium phosphate
USD	United States Dollar
WCA	Water Contact Angle
XPS	X-Ray Electron Spectroscopy

1. INTRODUCTION

1.1 Motivation

Bone is one of the major functional organs of the body that provide structural unity, load bearing, protection of internal organs, movement ability, blood production etc.[4]. Regardless of its location such as in the teeth or skull, any disruption to its structure can extremely affect the life quality of a patient. Thus, keeping bone functions healthy is quite important. With aging, bones become more brittle and lose their strength. Therefore, even minor accidents may cause severe injuries to bones of elderly people. Between 2015-2050, the world's population over 60 years is expected to increase from 12% to 22% [5]. With the aging population of world, metallic bone implants have been frequently utilized in the last decade. On the other hand, dental implants are widely used regardless of the patient's age. In 2024, dental implant market size is reported to be approximately 5 billion USD and approximately 10-15 million dental implants were used annually [6]. 61% of dental implants were made of Ti [7]. These figures indicate that Ti implants are the most commonly used implants that could replace and repair damaged parts of the bone. Biocompatibility is one of the crucial properties expected form a biomaterial. Along with the biocompatibility, osteointegration is the second most desired feature for bone implants. Basically, osteointegration is defined as contact between living bone and implant [8]. Stable support of prosthesis under loads, coherent motion between implant and surrounding tissues, compliance of new tissue with the implant should be considered together for the better understanding of osteointegration [9]. Low degree of osteointegration could end up with implant failure. For dental implants, early implant failure rates reported in literature are ranging from 0.7% - 7% [10],[11]. Following implant failure, reimplantation surgeries are usually required. Even though reimplantation has a relatively high success rate, the experience can be exhausting for some patients and causes economic burden on both patients and healthcare systems [12]. To enhance the osteointegration of implants, it's vital to understand the process. When a biomaterial is implanted in

the tissue, the surface of the biomaterial is immediately covered with water molecules, proteins and cells. Simultaneously, proteins arrange their conformation upon surface adsorption based on the surface properties. Composition, density and conformation of proteins mediate the initial cell linkage to the surface. Cells elongate their filopodia via integrins, which are cell surface receptors, to interact with extracellular matrix (ECM) proteins adhered on the surface. These receptor-protein clusters form focal adhesion points and eventually cells are attached to the biomaterial surface. Platelets releases signaling molecules which helps to attract monocytes, neutrophils and mesenchymal cells. Osteointegration is the formation of new bone tissue along with the implant surface. Cells do not directly interact with the surface, instead adsorbed protein layer strongly modulates their interaction. Hence, understanding the formation of protein layer and controlling their adsorption has great importance in biomaterial research [1],[13] . Surface properties such as roughness, wettability, charge and protein properties such as weight, conformation, hydrophilicity or hydrophobicity, surface charge is some of the vital parameters that mediate the protein adsorption. By modifying the surface properties, the amount of protein adsorption and their conformation can be observed. There are many surface modification techniques to choose from, depending on the material used and the purpose of the work. In this thesis, laser texturing was preferred to use for surface modification. Since their invention, lasers are being used in many industrial areas. In the health sector, they are frequently used in surgeries. Recently, they have been used as a tool for surface modifications. Hard biomaterials surface such as metals can be more easily modified by lasers. A desired pattern can be formed on the surfaces by using different laser sources, adjusting the beam duration, frequency and scanning speed. Upon interaction of laser beam with the material, the interacted point of surface is heated and evaporated by the energy delivery of the beam. Ultrafast lasers deliver energy to material in very short time interval thus, heated zone kept very small and created pattern become more precise [14]. High precision in patterns is the most advantageous aspect of laser texturing. Additionally, automatized laser set-ups provide reproducibility in terms of pattern. In this thesis, two different laser sources, femtosecond (fs) and microsecond (μs) laser, with different beam durations were used to form distinct periodic patterns on Ti samples. Femtosecond lasers and their intriguing laser induced periodic surface structures (LIPSS) pattern have at-

tracted great interest recently. It is already known that periodic submicron structures have positive impact on cell adhesion and proliferation. The main difference between fs and μs lasers is their pulse durations.μs lasers have longer pulse duration than fs laser and resulting in a wider heat damaged area around each pattern. With very short pulse duration (10^{-15} seconds), fs laser decreasing this heat damaged area while patterning the Ti surfaces. To observe the effect of the surfaces created by lasers with different operating principles, LIPSS structures and μs laser patterns which are already studied in our laboratory were textured on Ti samples [15],[16] . We aimed to investigate the effect of submicron sized patterns on protein adsorption and cellular behavior.

1.2 Objective

The main goal of this thesis was to investigate the impact of two distinct patterns on titanium samples done by different laser sources on protein adsorption amount, conformational changes of proteins, cell adhesion and proliferation. Periodic patterns which are known to be positively affecting osteointegration of biomaterial were formed by μs and fs laser treatments while preserving bulk properties of titanium. To further investigate the interaction of these patterns with proteins and cells in-vitro; protein adsorption and cell culture experiments were performed. Main objectives of this thesis were;

1. Forming distinct periodic patterns on titanium samples by μs and fs lasers.
2. Defining the surface properties such as wettability, roughness and topography using surface characterization techniques.
3. Comparing the protein adsorption amount and conformational changes of proteins upon adsorption on surfaces.
4. Investigating and comparing the cytotoxicity and cell proliferation of patterned titanium surfaces.

1.3 Outline

This thesis containing the chapters in the order of; Background about bone biology, biomaterials used as bone implants, laser treatment, mechanisms of protein adsorption and cell-biomaterial interactions. Material and Methods is presenting the experimental procedures. While Results chapter is containing the outcomes of experiments; Discussion is where all the results are analyzed and discussed. Lastly, Conclusion is summarizing the all deliverables and recommendations for future studies.

2. BACKGROUND

2.1 Bone Structure

Bone is a mineralized connective tissue, forming the skeleton and comprising 15% of the whole-body weight. Bony skeleton gives shape to the body, protects the internal organs, is responsible for blood generation, stores minerals such as calcium and phosphorus and secretes hormones. Bones are morphologically classified as long, short, flat and irregular bones [17],[18],[19]. Long bone is mainly composed of three types of structure; cortical bone, trabecular bone and bone marrow cavity. As names implies that the bone structures are mentioned accordingly how porous the structure or how densely bone is formed. Cortical bone, compact bone at the same time, is the denser outer part of long bones. These bones composed of many bundles called osteons. Each osteon is built up by a haversian canal where blood vessels are placed, lacunae where osteocytes are present, canaliculi as perforating canals between haversian canals and the hard matrix. Moreover, the blood vessels are interconnected to the vessels present at the outer surface of bone [17]. Cancellous, spongy or trabecular bone is less dense and more porous part of bone than cortical bone. It exists in the terminal and middle regions of the long bones [19].

2.2 Bone Cells

Bone tissue is comprised of four types of cells; osteoblasts, osteocytes, osteoclasts and bone lining cells. Each cell plays a different role in the bone formation and resorption processes. Osteoblasts and osteocytes are derived from mesenchymal stem cells while osteoclasts originate from hematopoietic stem cells such as blood cells. Even though they came from different origins, osteoblasts and osteoclasts are involved in similar processed such as activation of cells, bone formation-resorption and apoptosis. After their involvement in bone formation osteoblasts can differentiate into bone

lining cells to cover the bone surface or become embedded in mineralized bone matrix and differentiate into osteocytes. Non-differentiated osteoblasts are removed by apoptosis (programmed cell death) [20]. Osteoblasts are bone-forming cells with high capacity of protein secretion. They are mostly responsible from bone matrix production and bone mineralization. When osteoblasts are secreting collagen type I and other matrix proteins, they are forming osteoids. Osteoids are basically unmineralized bone matrix, additionally these structures are template for hydroxyapatite deposition [21]. Bone-forming and resorption are sequential events composing the bone remodeling for renewed bone tissue. Osteoclasts which are multinucleated cells differentiated from mononuclear hematopoietic stem cells are involved in bone-resorption stage of bone remodeling. In the guidance of cellular polarization, osteoclasts enable to attach the bone surface. They dissolve the mineralized matrix by acidification along the bone surface. Osteoclasts are undergoing apoptosis after the bone resorption. Moreover, osteoclasts produce factors named clastokines which control the osteoblast activity during the bone remodeling. Thus, osteoclast's mission is not only about resorption process, but also about the activity of other bone cells [19],[21]. Bone Lining Cells (BLCs) are flat shaped osteoblasts with low protein production capacity which are covering the bone surface. When osteoblasts differentiate into BLCs, the bone formation and resorption are terminated. Even though the features of bone lining cells are not precisely understood, these cells burden the direct interaction of osteoclasts and bone matrix, take a part of osteoclast differentiation and behave as osteoblast precursors in bone remodeling [22]. Osteocytes are mature osteoblast cells and they comprise 95% of total bone. After bone formation by osteoblasts, 5%-20% of osteoblast cells becomes enclosed into the bone matrix and mature into osteocytes. This differentiation transforms their morphology into more dendritic shape [23] Osteocytes are responsible of bone hemostasis which is the balance between formation and resorption processes. Function of osteocytes is mostly directed by both signaling and mechanical forces exerted on bone [24].

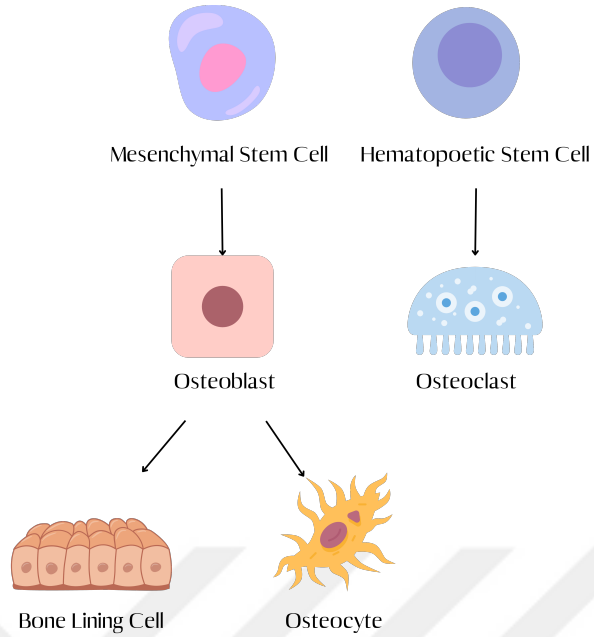

Figure 2.1 Illustration of bone cells draw by using Canva.

2.3 Biomaterials

Biomaterial is any substance used to repair or replace the any biological tissue or function in the body [25]. There are four types of biomaterials; polymers, metals, ceramics and composites. While polymers are divided as natural and synthetic polymer subgroups, ceramics are divided as bioactive, bioinert and bioresorbable ceramics. A biomaterial is mostly accepted as an implant due to the abundant clinical use. Moreover, one of the biomaterial definitions done at 1974, The 6th Annual International Biomaterial Symposium, is "a biomaterial is a systemically, pharmacologically inert substance designed for implantation within or incorporation with a living system" is suggesting the equivalence of implant-biomaterial definition [26].

2.4 Biomaterials Used for Bone Tissue

Polymers are organic compounds made up covalently bond long chain of monomers. For bone defects; natural polymers such as collagen, gelatin, alginate and silk are preferred biomaterials. Generally, these natural polymers are biocompatible and suit-

able for modification by adhesion ligands. However, most of the natural polymeric biomaterials have low mechanical strength. Because of the bone's load bearing features, a biomaterial designed to be used in bone tissue should have a balance between biocompatibility, bioactivity and mechanical properties. Synthetic polymers such as polyethylene glycol (PEG), polycaprolactone (PCL), polylactic acid (PLA) are suitable for chemical modifications. Therefore, it's easier to have more specialized and tailored biomaterials by using synthetic polymers. On the other hand, their cell adhesion and biocompatibility properties might not be as effective as natural polymer-based biomaterials [27].Bioceramics are a specialized class of ceramics used in biomedical field due to their biocompatibility, bioactivity and mechanical properties. Alumina, zirconia, hydroxyapatite, and bioactive glasses are the few examples of bioceramics. They are predominantly used as bone grafts or scaffolds, dental fillings, bioactive coatings and drug delivery systems. Bioceramics can be classified into 3 groups; bioactive bioceramics such as hydroxyapatite, bioresorbable bioceramics such as Tricalcium phosphate (TCP) that are resorbed by body and are replaced with natural tissue with time, biodegradable bioceramics such as polyglycolic acid (PGA) that are degraded into nontoxic byproducts. Metals are predominantly utilized for load-bearing applications such as artificial joints, spinal fixation devices, bone plates, bone screws, dental implants, and stents. Furthermore, metals are also used for their good electrical conductivity, as seen in applications such as cardiac pacemakers. Among the wide range of metallic biomaterials, some have become more prominent in the field including Co-Cr alloys, titanium and its alloys, stainless steel, gold and silver-based alloys [28]. Composites are materials mostly containing two or more phases together. These phases are named as matrix, primary material and reinforcement phases, often additives like particles or fibers to provide desired property to the material. Composites could be classified as polymer-based, ceramic-based and metal-based composites depending on the type of matrix material. Composite biomaterials preferably used in dental applications as bone substitutes or fillings and scaffolds for tissue engineering applications [29].

2.5 Titanium

Titanium (Ti) is a low-density metal with 4.5 g/cm^3 that is 60% lower than iron [30]. There are various grades of commercial titanium from Grade I to XIX that are alloyed with different metals at different ratios. One of the most abundantly used Ti as biomaterial is Grade II (commercially pure Ti) and Grade IV (Ti6Al4V alloy). As a biomaterial, Ti and its alloys are utilized as dental implants, bone plates and screws, stents and joint replacements etc. Ti demonstrates high corrosion resistance, enhanced biocompatibility, lower elastic modulus with high mechanical strength. Materials with higher strength and modulus than the natural bone, such as, 316L stainless steel (SS) and Co-Cr alloys could not transfer mechanical stress to the bone properly. This problem is named as stress shielding leading to bone resorption around the implant. Ti has lower elastic modulus varying from 55-110 GPa. Compared to 316L SS, with an elastic modulus of around 210 GPa or Cr-Co alloys, around 240 GPa; Ti exhibit more elasticity with similar mechanical strength [31]. In addition to that Ti is highly biocompatible material. It is neither show any toxic effect nor absorbed by body which is concluded in this article with the administration of 0.8 mg Ti to the human body [32].

2.6 Biomaterial-Tissue Interface

Surface is the first contact point of a biomaterial when it's implanted in the body. Events on implant-tissue interface are determining factor for implant failure [33]. At the interface, complex physical and chemical interactions are happening. It is complex and heterogenous environment consisting of many mineralized and unmineralized parts. In the context of bone-implant interface; osteoinduction, osteoconduction and osseointegration are important terms. Osteoinduction is the start of osteogenesis which means that pluripotent-stem cells differentiate into bone cells. Osteoconduction defines the biomaterials ability to enhance bone growth on its surface. Osseointegration is more like an umbrella term, embracing the aforementioned terms. It can be defined

as the integration of implant to bony tissue and tissue's outgrowth over the implant [34]. For the osseointegration of a biomaterial, protein adsorption and cell attachment are the two crucial biological activities.

2.7 Surface Modification

Numerous surface modification techniques have been developed to enhance biological response of body and to enhance a biomaterial's performance simultaneously. Enhancing protein adsorption, controlling the cell adhesion, proliferation, differentiation, and modulation of osseointegration are few examples demonstrating why surface modifications are required [35]. Surface modification techniques could divide into 2 subgroups; physical and chemical modifications. Chemical modification techniques are basically utilizing chemical grafting of functional groups to immobilize them onto the biomaterial's surface. Based on the used functional group; method name is defined such as silanization, fluorination or acetylation [36]. Physical modification techniques are less costly, safer in terms of application and more biocompatible than chemical modification. Nanoparticle assembly, simple physical adsorption, layer by layer assembly and co-electrospinning are few examples of physical techniques [36].

2.8 Protein Adsorption

Protein adsorption is non-covalently binding of proteins on the implant surface. It is a rapid and competitive event depending mostly on the inherit properties of protein and surface characteristics of biomaterial. Implantation of biomaterial have led to increase in interstitial fluid around the material which contains many plasma proteins. These proteins adsorb onto the biomaterial surface in seconds. Thus, biomaterial transformed to a recognizable entity for the body. Most of the time, cells are not directly interacting with the biomaterial. They recognize the biomaterial and interacts with it in the guidance of adsorbed protein layer. The sequential events of protein

adsorption and cell interactions with the implant are fundamental steps of Foreign Body Reaction (FBR) [37]. Cell interactions with implant would not be happen without protein existence.Therefore, analyzing and modulating protein adsorption along with biomaterial surface characteristics are vital in this research field. Protein adsorption is a complex phenomenon and affected by numerous parameters, however most important and understandable parameters could be listed as follows. Protein parameters affecting adsorption mechanism are;

- Protein composition
- Protein size
- Protein charge

Biomaterial parameters affecting adsorption mechanism are;

- Surface wettability
- Surface roughness
- Surface chemistry

Depending on the surface wettability, protein adsorption to surface and conformational changes upon adsorption can be altered. If a protein interacts with hydrophobic surface, hydrophobic residues of protein adsorb on the surface by disrupting the intra-protein interactions. Thus, entropy is increasing in protein structure. The increase in entropy became a guiding force for protein adsorption. While hydrophobic interactions are managing the protein adsorption on hydrophobic surfaces; van der Waals and electrostatic interactions are managing adsorption on hydrophilic and charged surfaces [13]. As another parameter, protein size has important role on adsorption mechanism. Smaller sized proteins are reaching earlier to a surface due to the higher diffusion exerted on them in blood stream. On the other hand, larger proteins adsorbed on surface

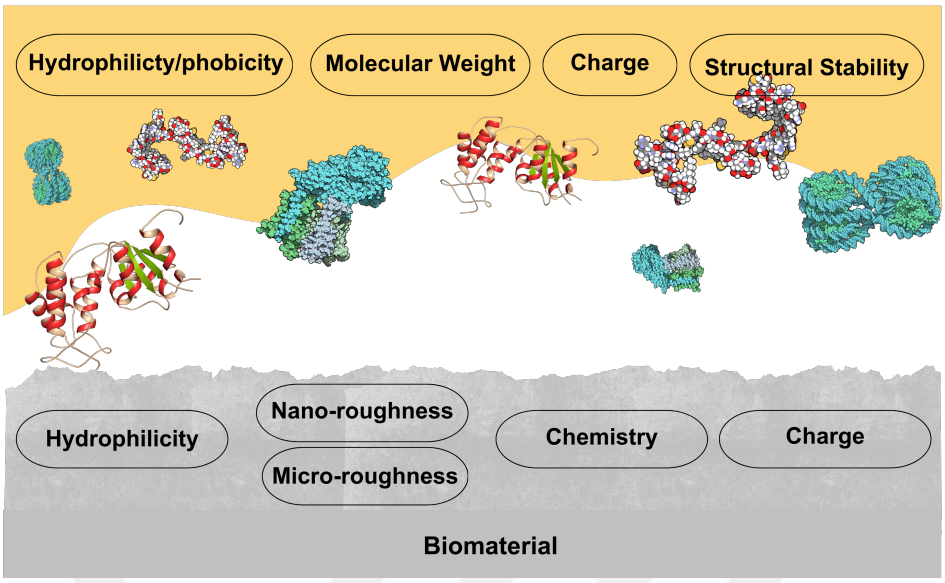

Figure 2.2 Summary of parameters affecting the protein adsorption mechanism draw by using Canva.

stronger than smaller ones. Therefore, when larger proteins arrive to the implant side, they moved the smaller ones and adsorb on biomaterial surface. This phenomenon is called as "Vroman Effect" [13]. From the biomaterial surface perspective; wettability, roughness, topography and surface charge are some of the important parameters. It has been reported that hydrophobic surfaces are more adsorb protein than hydrophilic surfaces [38]. Proteins adsorbing on hydrophobic surfaces are going under more conformational changes. It is well accepted that protein adsorption is not a phenomenon managed by only one parameter, but it is related to several parameters simultaneously. For example, surface hydrophobicity would not be enough for protein adsorption if surface and protein charges do not attract each other. From topographical perspective, increment of roughness means increment in the surface area. Therefore, rough surfaces may adsorb more proteins than smoother surfaces. Any surface modification for texturing may lead a change in surface chemistry. Then protein adsorption and conformation could be affected by surface chemistry, either. Thus, a comprehensive research is required to understand the guiding effects on protein adsorption.

2.9 Cell-Biomaterial Interactions

Cell biomaterial interactions are cell adhesion, spreading, migration and differentiation are crucial steps in terms of biomaterial integration. These interactions occur guidance of various molecular events such as protein adsorption. Most of the time, interactions between membrane proteins with the adsorbed proteins on biomaterial surface manage the cell-biomaterial interactions. Biomaterial implantation is resulting in a wound on tissue and initiated wound healing process composing of acute inflammation and formation of granulation tissue. In presence of non-biodegradable biomaterial such as titanium implants, fibrous capsule is formed around the material after granulation tissue is formed. Thickness of fibrous capsule is related to the biocompatibility of material. Thinner capsules are sign of more biocompatible biomaterial. However, acute inflammation step would be followed by chronic inflammation instead of capsule formation. Thus, the biomaterial is not biocompatible at all and the body is still trying to eliminate the foreign substance. In the better case scenario, fibrous capsule would not form since the biomaterial has porous or textured enough. Then the tissue ingrowths though pores or anchors on the textured surface [39]. Proteins directly undergo conformational changes when they adsorb on surface. This change can enable better cell attachment or inhibit it. In case of bone cell (osteoblasts) attachment and implants, fibronectin, laminin, vitronectin and collagen are the most important proteins. Integrins of osteoblast cells bind with adsorbed proteins on surface that can further triggers signaling pathways. Hence, proliferation and differentiation processes are initiated [38]. Various studies showing that rougher surfaces with nanoscale size patterns promoting osteoblast attachment [29],[30],[31].

2.10 LASER

Laser is a light source emitting nearly single wavelength photons in same phase. Spread of photon energy in undesired directions is negligible. Thus, laser beam is monochromatic, coherent and displaying least directionality. First ruby laser was in-

vented in 1960 by physicist Theodore Maiman. Following to this invention, in early 90s; Ar, Nd:YAG and Er:YAG lasers, in late 90s; Er, Cr:YSGG lasers were developed. Usage of lasers from soft and hard tissue ablation was enlarged into cutting of bone or dentin and removal of dental caries, recently. Furthermore, lasers have been extremely beneficial tool for surface modification of biomaterials thanks to its inherent features of depositing photon energy in a localized way to the surface [40] Laser-surface interactions could be analyzed under two aspects; laser ablation and laser interference. When a laser interacts with surface, it could ablate the surface due to photonic energy delivery. A focused laser beam irradiates the surface, extremely heats it and vaporizes the material from surface. This removal would be in micron-level precision therefore, micro-scaled topography could be patterned. On the other side, faster lasers interact with surface in very short duration of time that it permits periodic local heating of surface. Texturing based on laser interference has been used to fabricate nanoscale patterns. While micro and nanosecond lasers are working with the ablation principle; femto or pico-second lasers are working based on laser interference principle. The most fundamental difference between these lasers is the laser beam duration. Femto-second and pico-second lasers are ultrafast lasers; beam duration is approximately 10^{-12} and 10^{-15} seconds. In this case, thermal damage is very less, and localized energy intensity is high than laser ablation-based texturing [41].

2.11 Laser Surface Modifications

To modify texture of the surface, there are multiple methods have been applied so far. Sandblasting, acid etching and anodization are commonly utilized conventional techniques.However, these methods are forming irregular surfaces and controlling the irregularity technically is not possible. Moreover, methods like acid etching results in reduction in mechanical strength of the material [42].Besides, laser does not create significant changes in bulk properties of materials [40].Thus, laser assisted modification became prominent since laser devices provides the user controllable modification with keeping inherent material properties.Texture could be changed based on the change in laser power, frequency and laser beam duration (laser type).Laser texturing is more

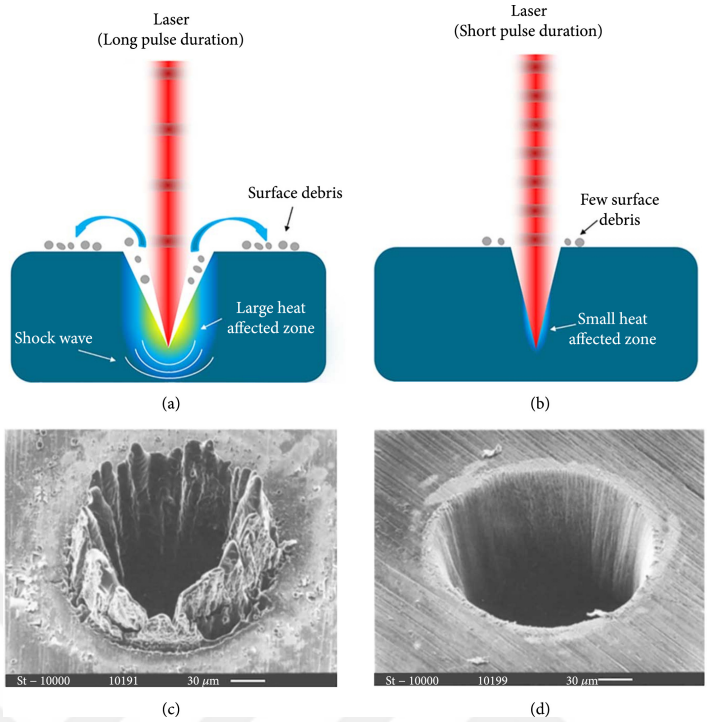

Figure 2.3 Illustration of long pulsed (a) and short pulsed laser (b) effect on surface. SEM images of laser ablated holes (c. nanosecond laser, d. femtosecond laser) on steel coil [1]

automatized process therefore, texture homogeneity is higher than other methods [41].

3. MATERIALS AND METHODS

The experimental set up composed of four parts; surface modification, surface characterization, protein adsorption experiments, and cell culture studies. For the surface modification and characterization; Scanning electron microscopy (SEM), Atomic force microscopy (AFM) and Water contact angle (WCA) were utilized to image the morphology, analyze the roughness and measure the wettability, respectively. The amount of protein adsorption was measured by using X-Ray photoelectron spectroscopy (XPS).The atomic ratio of N1s peak upon adsorption was used to compare the impact of surface pattern on adsorption [43],[44],[45]. Protein conformation upon adsorption was analyzed by means of FTIR spectra.For this purpose, peak fitting and deconvolution procedures were applied to the amide-I band (1700-1600 cm^{-1}). Changes in the percentage of area under the component peaks of amide-I band were representing changes in the secondary structure changes of the model protein, BSA, upon its adsorption on sample surface. Cell culture studies were conducted using two different cell lines; mouse fibroblast cells L929 (American Type of Culture Collection (ATCC), CCL 1, passage number 16) and mouse pre-osteoblast cells MC3T3-E1 subclone 4 (ATCC, CRL-2593, passage number 5). L929 cell line was used to analyze the possible cytotoxic effect of samples. On the other hand, MC3T3-E1 cell line was used to observe the proliferation of cells on differently textured surfaces. L929 cells were cultured with complete DMEM-F12 medium containing 10% FBS, 1% antibacterial/antimycotic solution; MC3T3-E1 cells were cultured with complete α-MEM medium containing 10% FBS, 1% antibacterial/antimycotic solution. According to ISO 10993-5 Biological evaluation of medical devices standard, there are several ways of analyzing the cytotoxicity of a biomaterials. Extract (Indirect) and Direct contact assays are two of it. Indirect MTT cytotoxicity assay was performed to evaluate the possibility of any release and formation of toxic substances after the laser process. On the other hand, Direct MTT Cytotoxicity assay was conducted accordingly ISO 10993-5 to assess the cytotoxic effect of samples when they are directly in contact with cells.

3.1 Preparation of Titanium Samples

1 mm thick Ti plates (Grade II, composed of %99 Ti with the least amount of iron (Fe), oxygen (O), carbon (C), nitrogen (N), hydrogen (H) [46]) were polished with silicon carbide polishing papers (P600, P1000, P2000 and P2500) and alumina powders (1 mm and 5 mm). Samples were cut from this polished Ti plates as 0.5 cm x 0.5 cm as square shape by means of modulated microsecond pulse fiber laser (JK400FGSI laser, UK, 1800 nm) [16].

3.2 Surface Modifications of Titanium Samples

There are 3 different surface patterns were textured on Ti sheets.First group was kept as polished sheets (pTi) which is explained under "Preparation of Titanium Samples" title. The second group (mTi) was patterned by microsecond pulse fiber laser (PALSS Laser, 400K, 1800 nm).The pulse length was 50 μs, operation frequency was 4 kHz and peak power was set to 95.6 W. The laser scanned the surface in x axis and created hemi-cycle like patterns following to the scanning direction.Third sample group (fTi) was patterned by lab-made femtosecond laser device (1030 nm)[47],[48]. The pulse length was 260 fs, repetition rate was 400 kHz and used average power was 1 W. The schematic representation of surface patterns of samples is demonstrated at Figure 3.1.

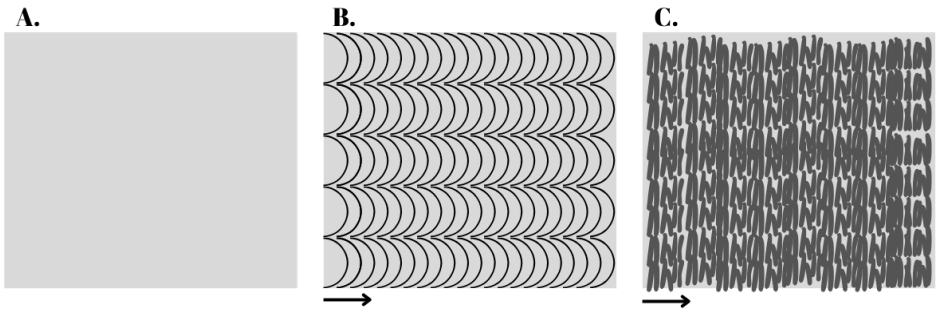

Figure 3.1 Schematic representation of modified Ti surfaces. A) pTi, B) mTi, C) fTi.

3.3 Surface Characterization of Ti Samples

3.3.1 Surface Topography

The surface topography of pTi, mTi and fTi samples were examined by means of SEM (Quattro ESEM, Thermo Fisher Scientific, US. Working distance for all images kept equal. The magnifications of each image were set as 1000x, 5000x, 10000x and 20000x.

3.3.2 Surface Wettability

WCA was measured through Contact Angle Measurement Instrument (CAM 100, KSV) by dropping 10 μL deionized water onto the sample surfaces. 3 replicates of pTi, mTi and fTi samples were imaged. These angles were measured through Image J Software (2012) via drop analysis plugin [2].

3.3.3 Surface Roughness

Surface topography profiles of micro and femtosecond laser textured Ti samples were taken by AFM (Nanomagnetics Veeco 5A, US) with tapping mode (using omcl-ac160ts 5m probe model).10 μm^2 and 50 μm^2 areas were scanned by AFM. 50 μm^2 scans were selected for analysis since greater area represents the general surface patterns better than smaller area scan. 3-D profiles, line profiles, height distribution and roughness parameters were calculated by using Gwyddion Software (2020).Each sample were analyzed through calculating the roughness mean square (S_q), average roughness (S_a), Kurtosis (S_{ku}) and skewness (S_{sk}) parameters in the software.

3.4 Protein Adsorption Analysis

3.4.1 X-Ray Photoelectron Spectroscopy (XPS)

Bovine serum albumin (BSA) adsorption on pTi, mTi and fTi samples was investigated by using XPS (Thermo Scientific K-Alpha, US). Each sample was incubated in 500 μL of 0.2 mg/mL BSA solution at 37°C for 10 minutes for achieving adsorption levels below saturation. Then samples were dried in furnace with the coverage of aluminum foil.Survey analysis was done prior to and following the protein adsorption on Ti samples to see the spectral differences. High resolution spectra of the N_{1s} regions were also obtained. The percentage of N_{1s} upon adsorption was used to compare the impact of surface pattern on protein adsorption [43],[44],[45]. The data were examined by means of CasaXPS (2023) software.

3.4.2 Fourier Transform Infrared Spectroscopy (FTIR)

Fourier Transform Infrared Spectroscopy (FTIR) (Thermo Fisher Scientific Nicolet is50, US) spectra was acquired to expose the secondary structure of proteins when they adsorbed on pTi, mTi and fTi samples. FTIR device was equipped with attenuated total reflectance (ATR) apparatus for this analysis. Samples were incubated in 1 mg/mL protein solution for 24 hours and gently washed with sterile deionized water, and air dried. 512 scans were collected for each sample by FTIR-ATR at a resolution of 4 cm^{-1}. The amide-I (1700-1600 cm^{-1}) region was further analyzed using OriginPro 2019 software (OriginLab Corporation, USA). Bands at around 1600 - 1700 cm^{-1} are assigned to amide-I band of proteins. To determine the secondary structure of the surface adsorbed protein, the amide-I band was further processed using the second derivative and curve fitting processes.The component peaks of amide-I band were identified using the second derivative (SD) and smoothing was performed using the Savitsky-Golay function with 5-9 points. Then a peak analyzer using the Levenberg-Marquardt algorithm was applied for curve fitting, Peak positions were not fixed during the fitting procedure.Band positions corresponding to specific secondary

structure components are pre-defined in the literature which is also summarized in the Table 3.1. [2],[3],[49].Then the percentage values of the different components were estimated by dividing the areas under each specific component band by the total area under the amide-I band.

Table 3.1
Deconvoluted amide-I band frequencies and assigned protein secondary structure components.Data are from [2], [3].

Assignment	**Mean Frequencies (cm^{-1})**
α-helix	1656 $\pm$ 2
β-Sheet	1624 $\pm$ 2 - 1642 $\pm$ 1 and 1691 $\pm$ 2 - 1696 $\pm$ 2
β turn	1667 $\pm$ 1 - 1680 $\pm$ 2
Intermolecular β sheets	1615 - 1630
Random Coils	1642 - 1657

3.5 Cell Culture Studies

3.5.1 Sample Preparation for Cell Culture Studies

One face of titanium samples was textured by fs and μs lasers. The non-textured back side of samples were coated and glued into the wells of 24 well plate by using poly-dimethysiloxane (PDMS). Samples were sterilized by immersing them in 70% ethanol for 15 minutes. After clearance of ethanol, samples were exposed to UV light for 30 minutes.

3.5.2 MTT Cell Cytotoxicity Assay

To assess the release any toxic substance from modified surfaces, the extract cytotoxicity procedure combined with MTT assay was applied. Additionally, direct MTT cytotoxicity assay were conducted to analyze any toxic effect when cells were directly in contact with sample surfaces [50].

3.5.3 Indirect MTT Cytotoxicity Assay

After the sterilization, 2 Ti samples from each experimental group were dipped into 4 mL of complete DMEM - F12 growth medium.The sample - growth medium amount was calculated according to the ISO 10993-12 [51].The growth media with titanium samples were incubated at 37°C for 72 hours to acquire extract growth medium solutions. Required amount of 100% extract solution was kept and the rest were diluted to 50%, 25% and 10% concentrations with complete DMEM - F12 medium. First, L929 cells were cultured on 96 well plate with using complete DMEM - F12 growth medium. After the incubation at 37°C, 5% CO_2 for 24 hours, complete growth media were replaced with extract growth media. Cells were kept in the extract growth medium for another 24 hours and MTT assay was applied. MTT assay was performed on 24th hour by adding 50 μL of 10% diluted 5 mg/mL MTT stock solution into each well. After 3 hours of incubation, MTT solution was aspired and formazan crystals in each well were dissolved by 100 μL dimethyl sulfoxide(DMSO). Absorbance were measured with a microplate reader (iMark Microplate Absorbance Reader, BioRAD Laboratories, CA, US) at 570 nm wavelength with reference wavelength of 750 nm.

3.5.4 Direct MTT Cytotoxicity Assay

3 x 10^3 cells/sample L929 mouse fibroblast cells were seeded on pTi, mTi and fTi with complete α-MEM growth medium (n=6). After 48 hours cultivation at 37°C, growth medium discarded and 500 μL of 10% diluted 5 mg/mL MTT solution in PBS were added into each well. Following a 3-hour incubation, MTT solutions were discarded, and 500 μL DMSO was added into each well. Well plates were placed on shaker for 10 minutes then the solution was transferred to 96 well-plate for absorbance reading. The microplate reader (iMark Microplate Absorbance Reader, BioRAD Laboratories, CA, US) at 570 nm wavelength with reference wavelength of 750 nm was used to measure the absorbance of solutions.

3.5.5 alamarblue Cell Proliferation Assay

5 x 10^3 cells/sample MC3T3-E1 mouse pre-osteoblast cells were seeded on pTi, mTi, and fTi samples with complete α-MEM growth medium. To assess the proliferation of cells on Ti samples, assay was conducted at 1th, 4th and 7th day of the experiment. Alamarblue solution (BioRAD Laboratories, CA, US) was diluted 10% with complete growth medium and 200 μL of diluted solution was added onto each sample following to aforementioned three days of experiment.When 3-hour incubation at 37°C was completed, reduced alamarBlue solutions were transferred to 96-well plate. Absorbance measurements were taken at 570 nm with 600 nm reference wavelength by means of a microplate reader (iMark Microplate Absorbance Reader, BioRAD Laboratories, CA, US). Acquired data were analyzed using the manual of the assay [51].

3.5.6 Evaluation of Cell Morphology

3.5.7 Scanning Electron Microscopy (SEM) Imaging

Cultivated cells were fixed on 7th day of experiment by 4% paraformaldehyde (PFA) solution for 30 minutes. The PFA solution was discarded and samples were rinsed with PBS twice. Following to the PBS wash, cells were gradually dehydrated with the use of 30%, 50%, 70%, 90% and 100% ethanol for 10 minutes incubation for each sample [52]. Afterwards, hexamethyldisilane (HMDS) was added on each well for drying the cells and samples were kept overnight under the hood. The SEM images were taken from 10 mm working distance under between 100X-200000X magnifications.

3.5.8 Fluorescent Imaging

Cell seeded Ti samples were fixed on 7th day of cultivation by 4% paraformaldehyde solution for 30 minutes. Afterwards, cells were permeabilized in 0.1% Triton-X for 5 minutes on gentle shaker. Following to the permeabilization, 1% BSA solution

including 0.1% tween-20 were used to block the cells. Actin filaments of cytoskeleton were stained with phalloidin (Alexa Fluor 488 Phalloidin, Thermo Fisher Scientific, MA, US). Working solution of phalloidin was prepared by diluting 15 μL of methanolic stock solution in 1% BSA solution (per ml). Sufficient amount of staining solution to cover the sample surface was added on each sample and kept for 20 minutes. For nuclear staining, DAPI solution was used which includes 4',6-diamidino -2 -phenylindole (DAPI) that strongly binds to adenine-thymine regions of DNA. Images were taken under blue excitation filter for F-actin filaments and violet excitation filter for nuclei. Since the Ti is non-transparent material, they were turned upside down to be imaged by the microscope (Leica DTC295). Acquired images were merged using Image J Software (2012) [53].

4. RESULTS

Protein adsorption, conformational changes and cellular behavior on pTi, mTi and fTi surfaces were investigated. Surface characterization was conducted by WCA measurements to investigate wettability; by AFM scans to investigate roughness of the surfaces. Adsorbed protein amount was analyzed by XPS and atomic ratios of elements present on BSA-adsorbed Ti surfaces. Protein's conformation upon adsorption was analyzed by FTIR-ATR based on area under the secondary structure component's peaks. Cellular behavior was investigated in terms of cytotoxicity and proliferation by conducting MTT and Alamarblue assays using L929 fibroblast and MC3T3-E1 pre-osteoblast cells, respectively.

4.1 Material Characterization

4.1.1 Investigation of Ti Surface Patterns

pTi, mTi and fTi samples were imaged by using SEM. Working distance was kept fixed for each image. Samples were imaged at 1000x, 5000x, 10000x and 50000x magnifications. The images are shown on Figure 4.1. pTi samples were only polished and do not have specific pattern. mTi samples were patterned by microsecond laser and parallel hemicycle like patterns in x axis were formed. fTi samples were patterned by femtosecond laser and laser induced periodic surface structures (LIPSS) were formed on the surface.

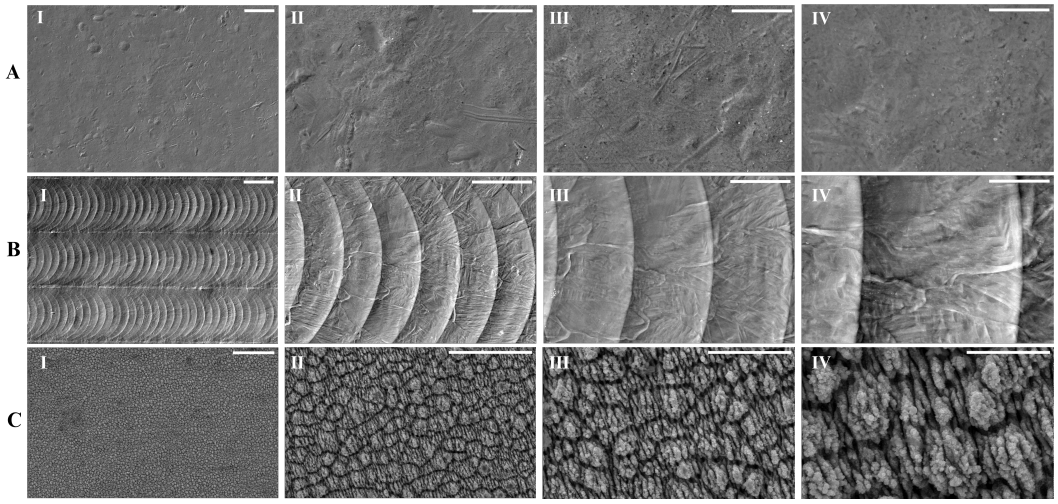

Figure 4.1 SEM images of Ti samples. A) pTi, B) mTi, C) fTi. Scale bars from left to right; 50 μm, 20 μm, 10 μm and 5 μm.

4.1.2 Water Contact Angle Measurement (WCA)

The WCA values and representative images for the WCA measurements images are shown in Figure 4.2. The WCAs were calculated as 54.36±3.76°, 73.55±6.04° and 113.60±13.49° for pTi, mTi and fTi, respectively.

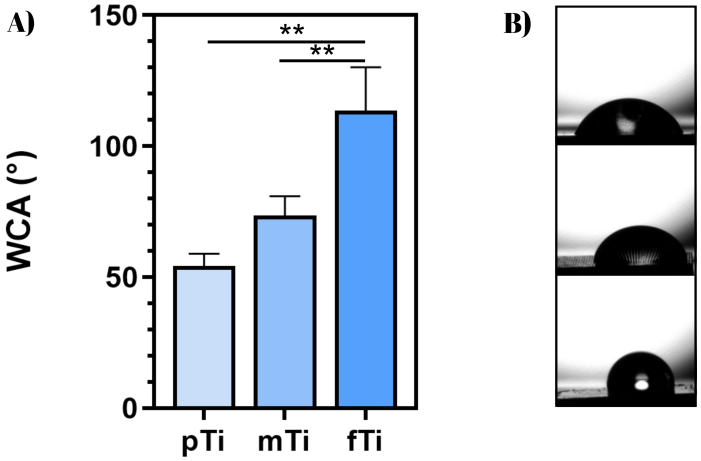

Figure 4.2 Water contact angle measurements of pTi, mTi and fTi surfaces. B) Images of water droplets from top to down is; pTi, mTi and fTi. Error bars representing the standard deviation.

4.1.3 Atomic Force Microscopy Measurements (AFM)

Surface topography was imaged, and the surface roughness measured using AFM imaging. Images were obtained from 50 μm x 50 μm area. The 3D illustration of the surfaces, surface profiles, and surface height distribution were obtained using Gwyddion software and presented in Figure 4.3. The values of the surface root mean square (S_q), average roughness (S_a), surface skewness (S_{sk}) and surface kurtosis (S_{ku}) are given in Table 4.1. (S_q) and (S_a) values showing that the laser texturing increased surface roughness. (S_{ku})=3 represents the Gaussian height distribution function which is only showed by pTi group. (S_{ku})$<$ 3 is represents fewer extreme height variations such as the surface of mTi and fTi.

Table 4.1
The roughness values of Ti sample surfaces calculated from AFM analysis.

Groups	**S_q (nm)**	**S_a (nm)**	**S_{sk}**	**S_{ku}**
pTi	71.58	53.99	-0.18	3.31
mTi	200.50	155.00	-0.31	0.86
fTi	422.50	328.80	0.16	0.72

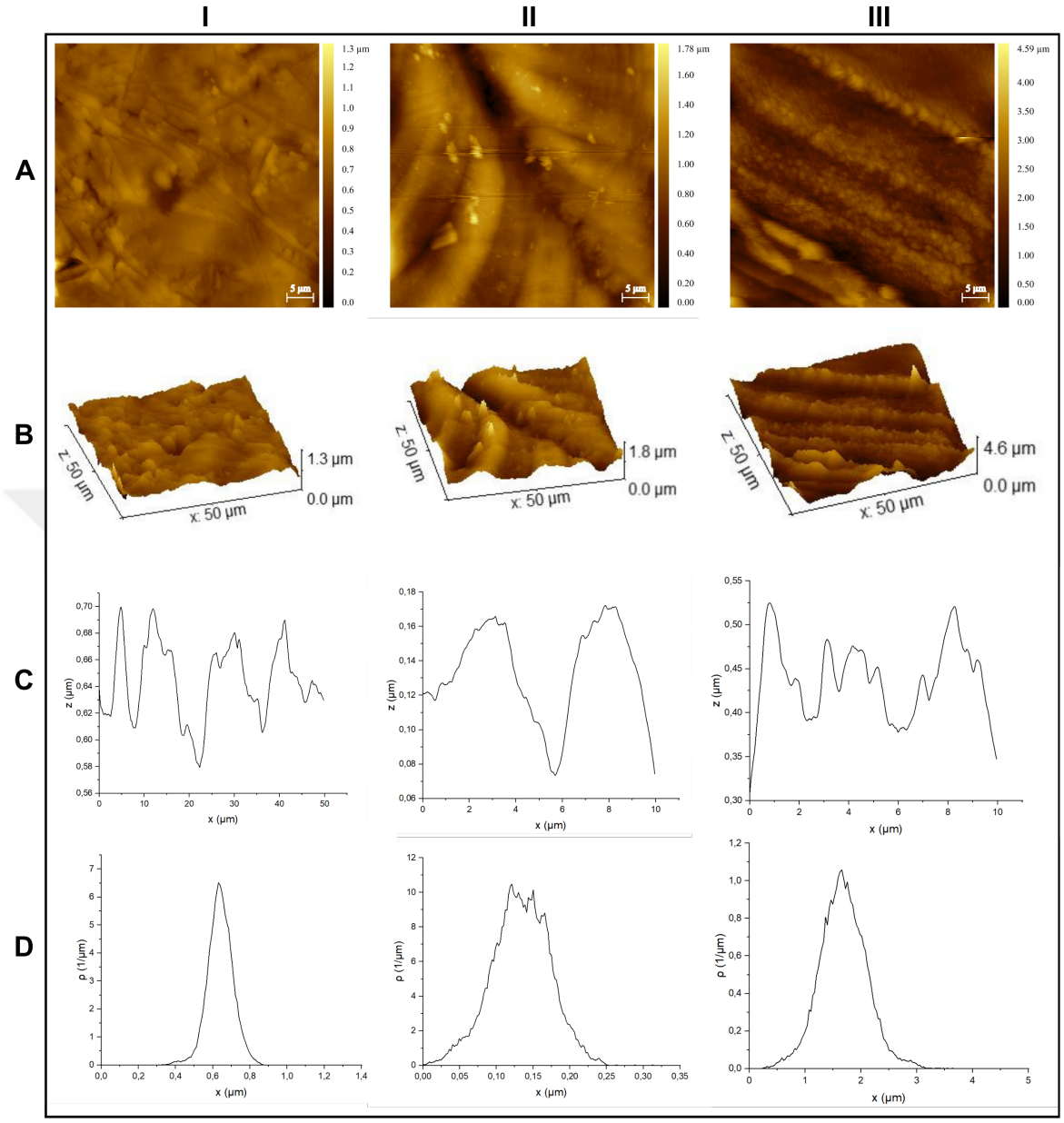

Figure 4.3 Roughness parameters of I) pTi, II) mTi and III) fTi samples. A) AFM images were taken in area of 50 μm x 50 μm. Scale bars show 5 μm distance. B) 3D profiles of the samples. C) Line profiles of titanium samples. D) Height distribution graphs of the samples.

4.2 Protein Studies

4.2.1 X-Ray Photo-electron Spectroscopy (XPS)

The amount of surface adsorbed protein was estimated via XPS. A survey scan was performed prior to and following protein adsorption on the sample surfaces. The XPS spectra are presented in Figure 4.4. A. High resolution spectra of Ti_{2p} and N_{1s} peaks of protein adsorbed surfaces are presented in Figure 4.4. B. and Figure 4.4.C. Atomic ratio of elements for bare and protein-adsorbed and non-adsorbed are presented in Table 4.2. Protein adsorbed surfaces showed increased N_{1s} peak intensity while the intensity of Ti_{2p} peaks decreased upon protein adsorption. Atomic percentage of N_{1s} was utilized to compare the adsorbed BSA amount on Ti surfaces. Based on N1s, protein adsorption amounts were ordered as pTi > mTi > fTi.

Table 4.2
Peak Positions and Atomic Ratios of Elements on the BSA-adsorbed Ti Samples

	Peak Positions (eV)				**Atomic Ratio of Elements (%)**			
Samples	**C_{1s}**	**N_{1s}**	**O_{1s}**	**Ti_{2p}**	**C_{1s}**	**N_{1s}**	**O_{1s}**	**Ti_{2p}**
pTi	286.08	401.08	532.08	459.08	59.10	7.59	31.70	1.61
mTi	287.08	402.08	534.08	460.08	56.95	7.33	35.33	0.40
fTi	283.00	398.00	529.00	456.00	52.84	4.80	40.99	1.37

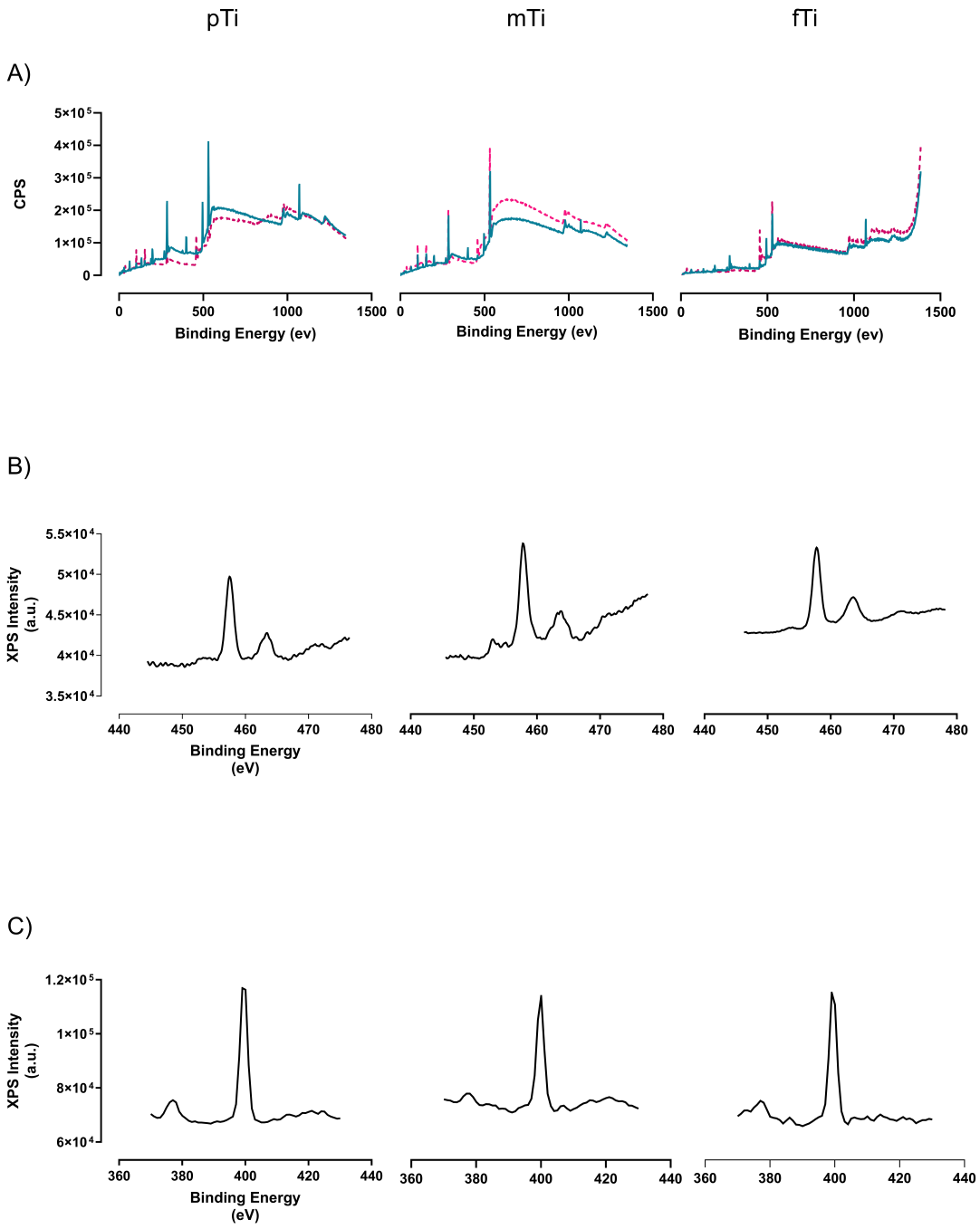

Figure 4.4 XPS Analysis of protein adsorption on Ti samples. A) Survey spectra of Ti surfaces. Teal colored line is demonstrating peaks following to the protein adsorption while pink colored line showing the peaks prior to the protein adsorption. B) Ti_{2p} high resolution spectra of pTi, mTi and fTi surfaces upon protein adsorption. C) N_{1s} high resolution spectra of pTi, mTi and fTi surfaces upon protein adsorption.

4.2.2 Fourier Transform Infrared Spectroscopy (FTIR)

Changes in secondary structures of BSA upon surface adsorption was analyzed using the amide-I band. When peaks were deconvoluted, the bands at around 1624±2 - 1642±1 cm⁻1 and 1691±2 - 1696±2 cm⁻1 region were assigned to β-sheet, 1667±1 - 1680±2 cm⁻1 to β-turn, 1615 -1630 cm⁻1 to intermolecular β-sheets, 1656±2 cm⁻1 to α-helix and 1642 - 1657 cm⁻1 random coil folding, whic is also shown in Table 4.3. The amide-I band and secondary structure components are shown in Figure 4.5. A component peak at around 1666 cm⁻1 was neglected in the calculations. Area under the curve of each component calculated and shown in the Table 4.4.

Table 4.3
Wavenumbers of BSA secondary structure upon adsorption on pTi, mTi and fTi surfaces. (NA: Not announced. "- ": not exist in native BSA structure

	pTi	mTi	fTi
Secondary Structure	**Center Wavenumber (cm^{-1})**	**Center Wavenumber (cm^{-1})**	**Center Wavenumber (cm^{-1})**
α-helix + random coil	1649	1649	1647
Intermolecular β-sheet	1613	NA	NA
β-turns	1678	1681	1681
β-sheet	1627	1622	1622

Table 4.4
Percent Area of BSA secondary structure upon adsorption on pTi, mTi and fTi surfaces. (NA: Not announced. "- ": not exist in native BSA structure

	Native BSA [63]	pTi	mTi	fTi
Secondary Structure	**Percent Area (%)**	**Percent Area (%)**	**Percent Area (%)**	**Percent Area (%)**
α-helix + random coil	69.0	61.6	81.2	81.3
Intermolecular β-sheet	-	4.7	NA	NA
β-turns	4.0	10.1	8.0	8.1
β-sheet	14.0	22.7	10.5	10.4

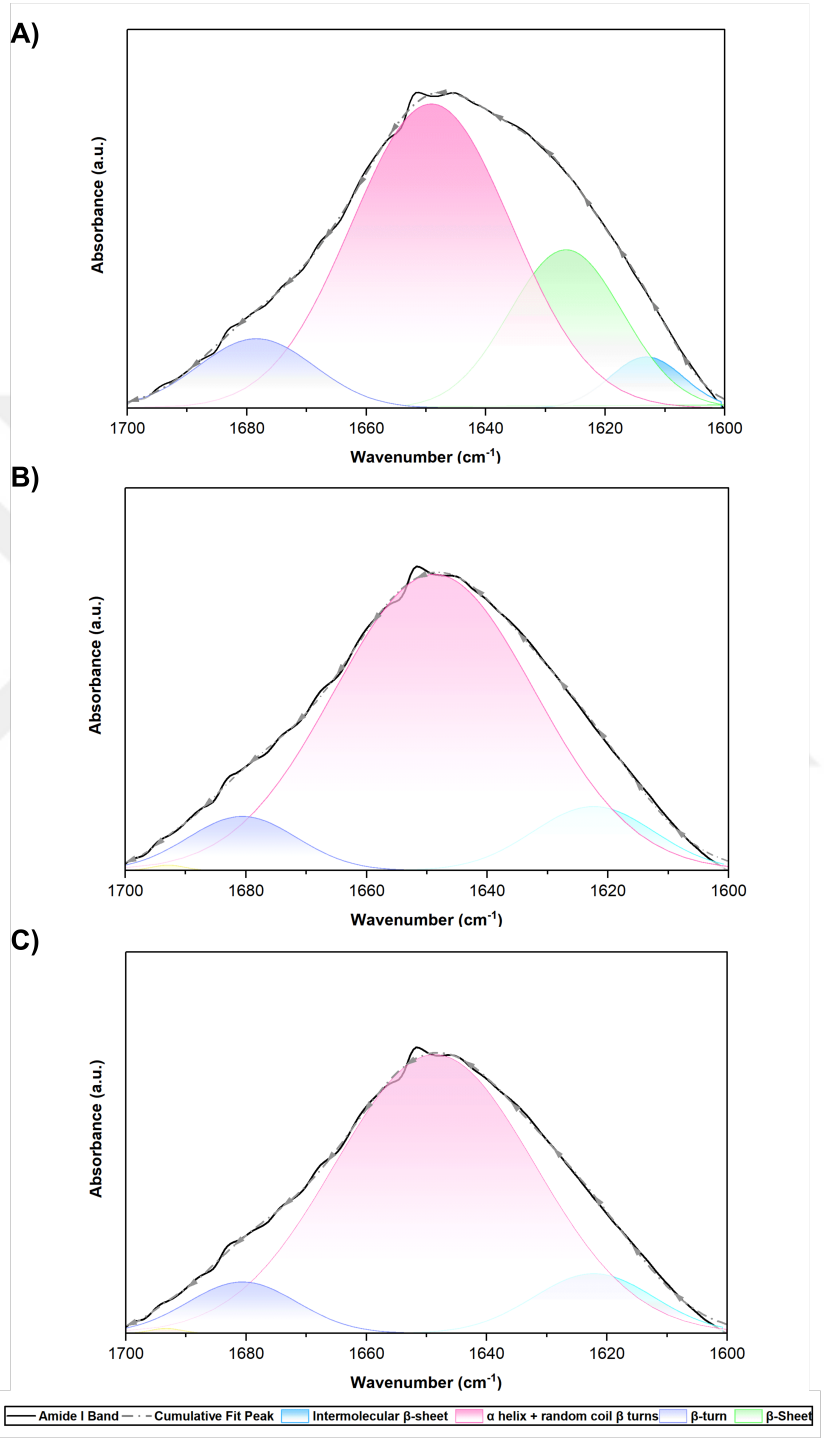

Figure 4.5 amide-I band of BSA at 1645 cm^{-1} on A) pTi, 1651 cm^{-1} on B) mTi and 1645 cm^{-1} on C) fTi samples with deconvoluted peaks of secondary structure components

4.3 CELL CULTURE STUDIES

4.3.1 Indirect MTT Cytotoxicity Assay

Indirect MTT assay was done using the extract growth media. Mean cell viability of indirect MTT assay of samples were 315.02±36.7%, 325.37±33.9%, 285.97±22.0%, 100±9.9% and 51.34±5.42% for pTi, mTi, fTi, PC and NC, respectively. There is significant difference between cell viabilities of pTi, mTi, fTi and positive control group. However, there is not a significant viability difference between pTi, mTi and fTi groups. Results shown in Figure 4.6A.

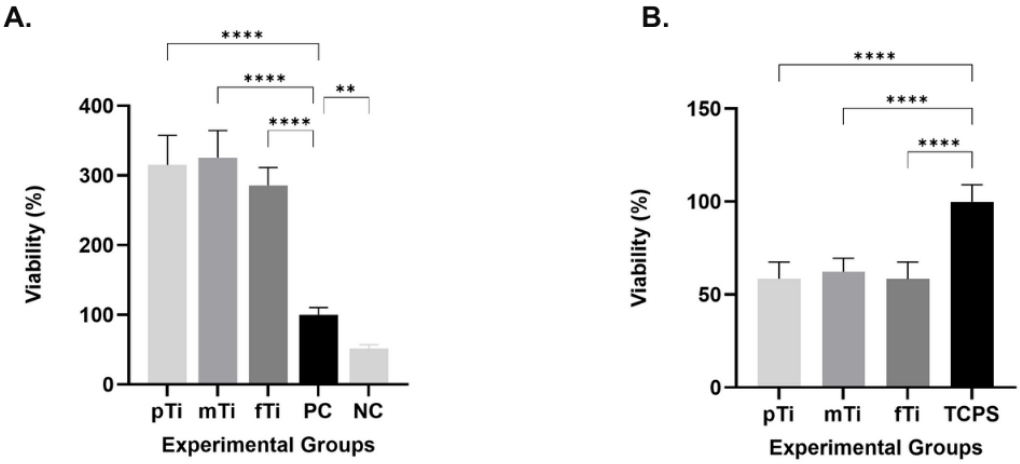

Figure 4.6 A) Results of Indirect MTT cytotoxicity assay of L929 fibroblast cells on pTi, mTi, fTi, PC and NC surfaces. (PC: positive control, NC: negative control) B) Results of Direct MTT cytotoxicity assay of L929 fibroblast cells on pTi, mTi, fTi and TCPS. (TCPS: Positive control.) (**:$p<0.01$) (****:$p<0.0001$)

4.3.2 Direct MTT Cytotoxicity Assay

L929 cells were directly seeded on Ti samples to conduct the direct MTT cytotoxicity assay. Mean cell viability of direct MTT assay results were 58.57±9.03%, 62.31±7.22%, 58.38±9.20% and 100±9.06% for pTi, mTi, fTi and TCPS, respectively. Cell viability is significantly decreased compared to the TCPS. Figure 4.6.B shows the results of direct MTT assay.

4.3.3 alamarBlue Cell Proliferation Assay

MC3T3-E1 rat pre-osteoblast cell proliferation was analyzed using alamarBlue assay. Assay was conducted on 1st, 4th and 7th day of cell incubation. Only the results from of the 7th day were compared statistically to see the highest difference in cell proliferation since the aim was observing the cell proliferation on longer periods as it does in real cases. Normalized cell proliferation to day 1 TCPS is 68.55±2.25% for pTi, 72.49±2.71% for mTi, 78.66±4.05% for fTi and 120±2.81% for TCPS at the day 7. Cell proliferation was significantly different between the experimental groups (pTi, mTi and fTi) compared to positive control (TCPS). Between Ti samples, fTi has shown significantly higher proliferation rates than pTi ($p<0.0001$). There was also statistically significant difference between cell proliferation on mTi and fTi groups ($p<0.05$). Results are shown on Figure 4.7.

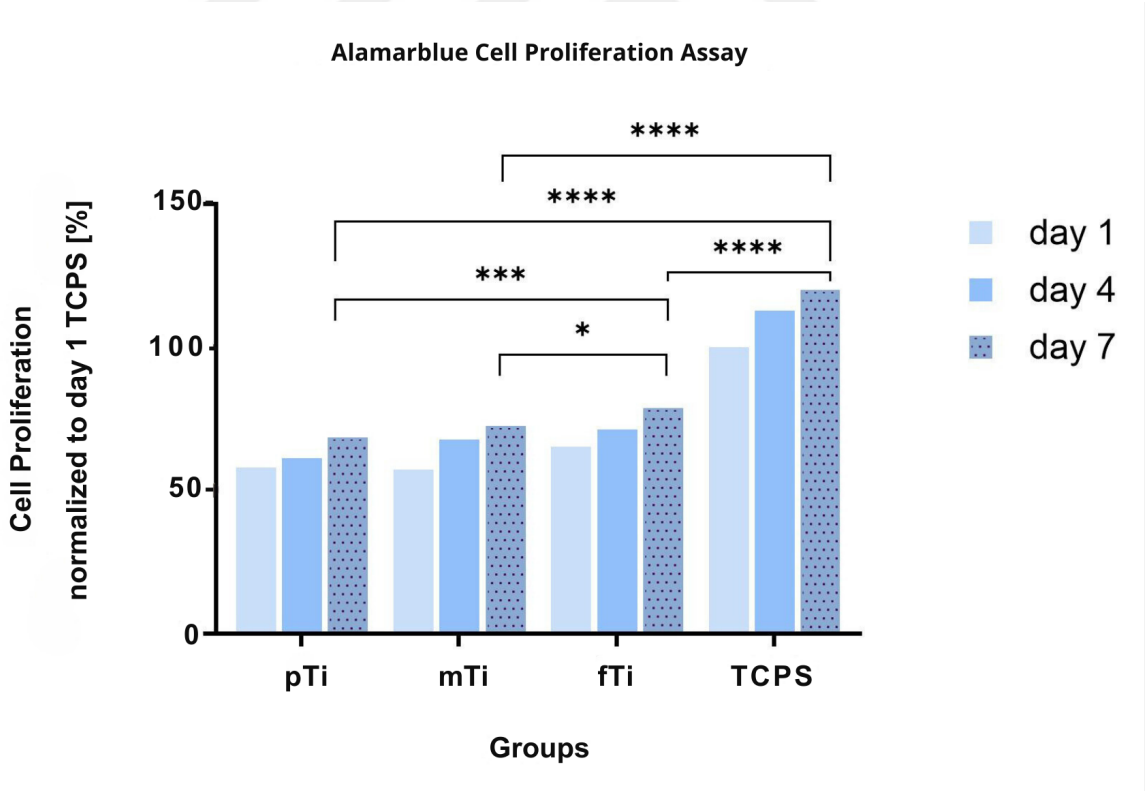

Figure 4.7 alamarBlue cell proliferation assay to assess the effect of MC3T3-E1 proliferation on the pTi, mTi and fTi surfaces. (*: $p<0.05$, ****: $p<0.0001$) (TCPS: positive control)

4.3.4 Morphology of MC3TC3-E1 Cells

The morphological assessment of MC3T3-E1 cells were evaluated by using SEM, in Figure 4.8. According to the SEM images, MC3T3-E1 cells formed more contact points with elongated shape on mTi and fTi compared to pTi. MC3T3-E1 cells on pTi are attached to surface predominantly by means of lamellipodia which are demonstrated by ruffled membrane edges. Along with lamellipodia formation, cells on the mTi and fTi surfaces are displaying more filopodia structures than the pTi.

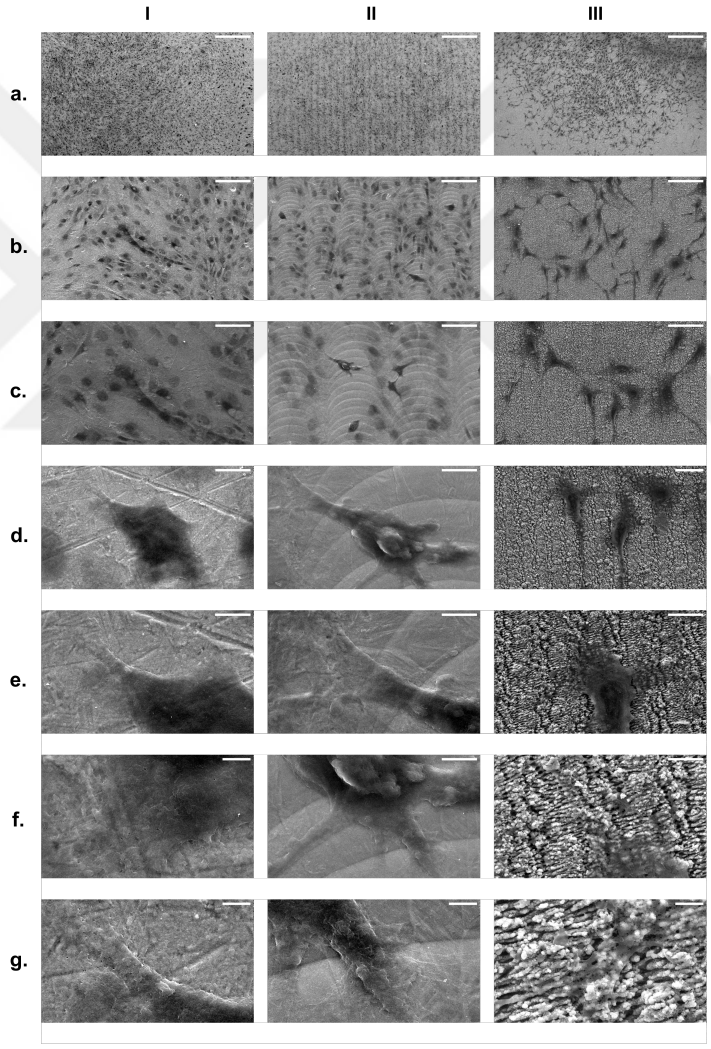

Figure 4.8 SEM images of MC3T3-E1 pre-osteoblast cells on I) pTi, II) mTi, III) fTi samples. Cells were imaged with a. 100X b.500X c.1000X d.2000X e.5000X f.10000X g.20000X magnifications. In the same order, scales bars are demonstrating 500 μm, 100 μm, 50 μm, 20 μm, 10 μm, 5 μm and 2 μm distance.

4.3.5 Fluorescent Staining

The effect of pattern on cell spreading and alignment were investigated by staining the actin cytoskeleton and nuclei localization of MC3T3-E1 cells, using phalloidin and DAPI staining solutions respectively. Images were taken on the 7th day of incubation could be seen on Figure 4.9.

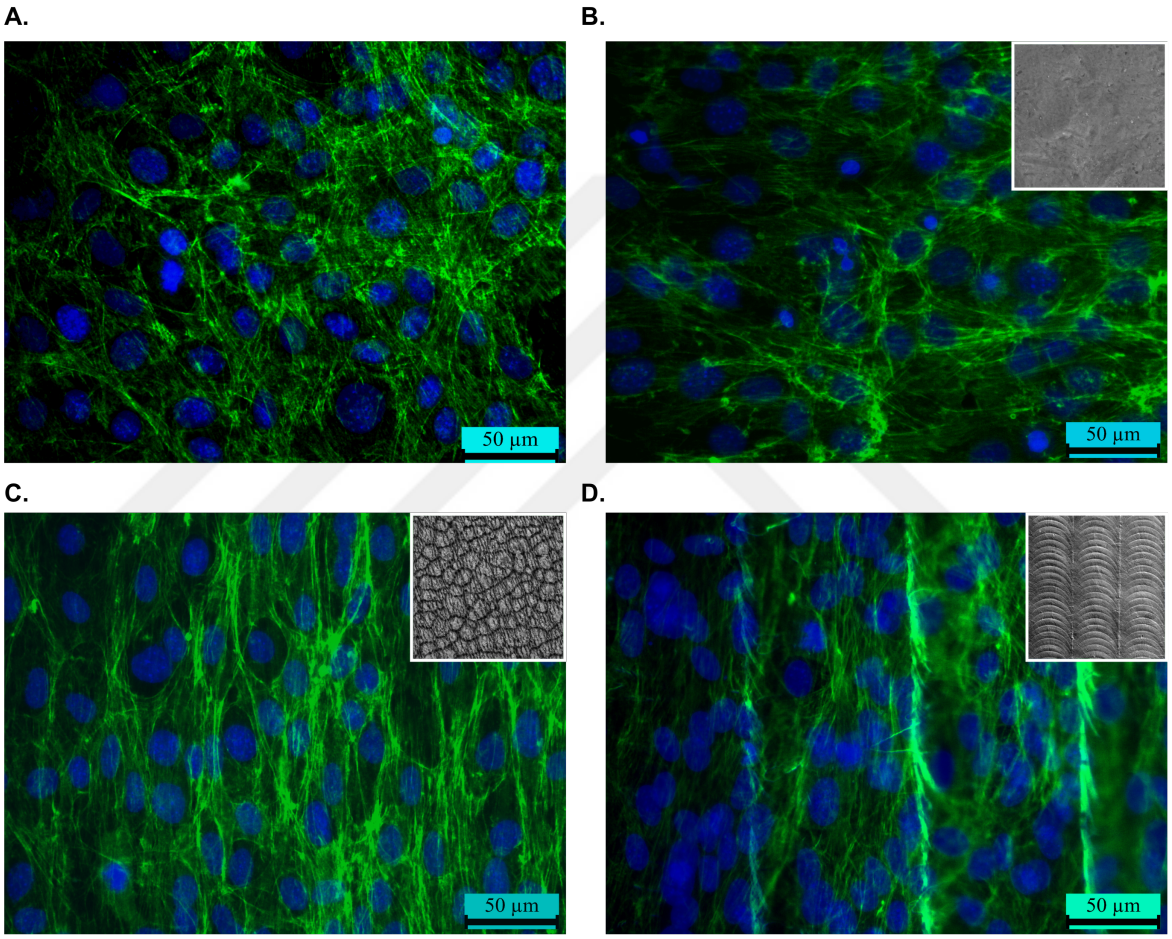

Figure 4.9 Nuclear (DAPI) and actin skeleton (Phalloidin) staining of MC3T3-E1 cells on Ti samples. A) TCPS:positive control, B) pTi, C) fTi, D) mTi. The surface patterns are shown on the upper inlet SEM photos of corresponding Ti samples.

4.4 Statistical Analysis

All statistically significant differences mentioned throughout this thesis were determined using one-way ANOVA with post-hoc Tukey's honest significant difference test where $p<0.05$ was considered to show meaningful statistical difference.

5. DISCUSSION

5.1 Material Characterization

Periodic submicron patterns were formed using microand femto-second lasers on titanium surfaces. Laser texturing allows the researchers to make controllably tune the surface properties such as roughness, wettability, corrosion resistance or hardness [64]. Conventional surface modification techniques such as acid etching, anodic oxidation, grit blasting is also used to create periodic surface pattern. However, these techniques have low reproducibility and low pattern precision compared to laser texturing. Laser texturing have been used to enhance friction coefficient and wear resistance of material and to promote osteointegration which is reported in the literature [40],[41]. In this thesis, two different laser sources; μs laser and fs laser were utilized for surface modification. As an outcome of μs and fs laser texturing, hemicycles-like patterns and LIPSS structures were formed on Ti, respectively. The result of LIPSS period is supported by findings of Bonse *et. al* reporting that the LIPSS formation on metals are predominantly results in low spatial frequency (LSFL) LIPSS [54]. Laser texturing is affecting the wettability depending on laser parameters is reported in the literature [55]. Water contact angle values increased in mTi and fTi surfaces after laser texturing [56]. Same Grade II Ti sheets was used in the study of Akkan *et. al* and WCA was measured as 65.5$\pm$0.8° and by polishing its decreased to 24.6$\pm$0.6°. The same procedure described by Akkan et.al was followed for polishing, WCA is decreased to 54.36$\pm$3.76° in our case. The same procedure was followed to pattern mTi surfaces; similar to Akkan *et. al* study, we also observed an increase in WCA of mTi samples [57].For LIPSS structures, 113.60$\pm$13.49° WCA is consistent with WCA ranges reported in literature [58],[59]. The reasons behind the increase in WCA could be the increase in roughness of the surfaces. Kietzig *et.al* are stating that the Wenzel's equation about increasing roughness increases hydrophilicity of inherently hydrophilic structures could not explain the hydrophobicity of LIPSS [60], [61] .In Figure 4.3, AFM scans over 50 μm x 50 μm area are given with their 2D, 3D illustrations, horizontal height profiles taken from

the center of the image, and height distribution functions. Horizontal height profiles taken from the center line shows that pTi surfaces have random surface morphology and relatively narrow height distribution. Height distribution graphics are representing the frequency of heights of the surface. Narrow variation on x axis on the pTi group indicates a smoother surface with clustered height values around a mean value. The height distribution value of the mTi surface shows greater height variation. However, when examined numerically, the range of the x axis is seen to be between 0 -0.25 μm, while the range of the x axis for fTi is between 0 -3 μm. Thus, fTi surface is composed of deeper holes and sharp peaks with almost homogeneous distribution on surface. Since the peak shape resembles the Gaussian peak but the variation on x values are greater than height distribution graph of mTi pattern. It should be noted that the AFM scans of mTi pattern were taken at the intersection of two hemicycles. Thus, it might not be representing the whole surface roughness properly. Further analysis with multiple scans from different points of the surfaces would better explain the surface profile. Most studies describing the surface roughness by using only root mean square (RMS), S_q, value which is easily calculated from AFM images. S_q is representing the height fluctuations of surface height values around the mean height. Therefore, surfaces with very different topographies may have similar S_q values. In this thesis, in addition to the S_q value, surface topography is analyzed by using additional roughness parameters such as skewness, kurtosis, average roughness for better describing the topography [62]. The equation of RMS parameter includes the squares of surface height deviations, therefore S_q is more affected by outlier values. S_a is basic arithmetic mean calculation of surface and gives us a general view of surface roughness. S_a and S_q showed that the laser texturing increased the roughness of mTi and fTi surfaces as most of the studies reported in literature [63]. pTi and mTi have negative S_{sk} values which indicates height distribution function leaning to smaller heights and predominant valleys. fTi has a positive S_{sk} value representing pointed elevations rather than flat areas. pTi surface shows the most sharpness with 3.3 nm S_{ku} in terms of height profile resembling a Gaussian distribution. Thus, height values distributed in flatter manner around the mean. These values are compatible with SEM (Figure 4.8) and AFM (Figure 4.3) images [43],[63].

5.2 Protein Adsorption Studies

BSA was used as the model protein for the protein adsorption studies since albumin is one of the most abundant proteins in the blood. Additionally, BSA is structurally similar to human serum albumin (HSA) and commercial BSA is low cost and easy to purchase [64]. Relative amount of BSA adsorbed on Ti surfaces was investigated by means of XPS [43] Atomic percentages of nitrogen (N) present on the surfaces upon BSA adsorption were compared among the Ti surfaces. According to the results, the amount of BSA adsorbed on pTi surfaces was higher followed by mTi and fTi surfaces. It's known that protein adsorption is affected by protein's intrinsic features and surface chemistry, wettability and morphology in general [13] . It's reported by many studies hydrophobic surfaces induce more protein adsorption along with greater denaturation [65],[66]. In this thesis, the surface with relatively high hydrophilicity resulted in the highest BSA adsorption amount. BSA is a soft protein and easily changes its structure to adhere the all surfaces either hydrophilic or hydrophobic which can explain its adsorption on the hydrophilic pTi and mTi surfaces [82]. Laser texturing increased the oxygen amount on the surface which is also creating negatively charged environment on the Ti surfaces at pH 7. BSA is negatively charged at pH 7 as well [67]. Same charges would end up with negative repulsion between BSA and mTi, fTi surfaces. According to the results in Table 4.2, fTi surfaces has the highest O1s ratio (56.2 %) compared to pTi (40.73%) and mTi (52.68%). This might have led to less BSA adsorption on fTi surfaces than mTi and pTi surfaces. It should be noted that XPS analysis might not reflect the exact amount of BSA adsorbed on fTi, since sampling depth for XPS is accepted as 10 nm or less and according to the AFM results (Figure 3.3), fTi surface has 4.6 μm depth which is significantly higher than XPS sampling depth [68]. Hence, adsorbed BSA in the pits of fTi pattern may not be detected by XPS. Upon adsorption on the Ti surfaces, conformation of the proteins changed based on interactions with the surface. Wettability and roughness have significant effect on conformational changes [69],[70]. In aqueous solution, secondary structure of BSA contains approximately 53% α-helix, 14% β-sheet, 4% β-turn and 16% random coils. Generally, the position of the amide-I band is centered at around 1655 cm^{-1} and it can shift down to lower wavelengths as the number of random coils increases [71]. The amide-I band

maxima were observed at 1645 cm^{-1} for pTi, 1651 cm^{-1} for mTi and 1645 cm^{-1} for fTi surfaces indicating that random coils increased upon BSA adsorption to these surfaces. Upon adsorption to mTi and fTi surfaces in very similar conformational changes were observed in the secondary structure of BSA. α-helix and random coil structures was increased approximately 12% while β-turns increased 6% relative to the native BSA structure. Additionally, 10% β-sheet was observed on both laser textured surfaces. All these changes supports the literature findings that the wettability and roughness caused conformational changes in BSA structure upon adsorption [69],[70], [72] . BSA was significantly resulted in the all three sample groups but laser texturing resulted in the highest denaturation on BSA structure. As its stated in the studies on protein adsorption, its more correct to consider the combined effect of the parameters. Based on the results of this thesis, increased hydrophobicity and roughness did not enhance the protein adsorption while resulted in the higher protein denaturation in same experimental groups, mTi and fTi. While the effect of nano-roughness on conformational changes is directly observed, its effect on the amount of adsorption can be explained by its connection with hydrophilicity.

5.3 Cell Culture Studies

Cellular cytotoxicity was assessed by using L929 mouse fibroblast cells according to the ISO 10993-5 standard. L929 fibroblast cells are one of the highly preferred cell lines for the cytotoxicity assays since mouse fibroblast cells are more sensitive to toxic content than human fibroblast cells [73]. According to the Indirect MTT assay results, all Ti groups resulted in higher cell viability compared to positive control. Among Ti groups, there was not a significant viability difference. Thus, polishing and laser texturing on Ti groups did not release any cytotoxic substance into the extract growth media. Mean cell viability of direct MTT assay results were 58.57±9.03%, 62.31±7.22%, 58.38±9.20% and 100±9.06% for pTi, mTi, fTi and TCPS, respectively. According to the direct MTT assay outcomes, there are significant viability decrease in Ti groups compared to TCPS. Decrease in the viability is not less than 30%. Thus, the patterned Ti surfaces demonstrated cytotoxic effect according to ISO 10993-5 standard.

In the literature, roughness value up to a level was enhancing the L929 viability but excessive roughness inhibits cell adhesion to the surface and causes the cell death. There is not a defined threshold for the roughness but relative comparison between rough and smooth surfaces reported that fibroblast viability was higher on the smoothest surface [74]. Cell proliferation on Ti samples were analyzed via alamarBlue assay. After 7 days, all three Ti groups represented similar upward trend in cell proliferation. Even though, all surfaces are seen to be appropriate for cell growth, Ti samples displayed reduced cell proliferation than TCPS which is also encountered in the literature [75]. The highest proliferation rate among Ti groups was showed by fTi. The basic difference between these experimental groups is the roughness values (S_a of pTi is 53.99 nm, mTi is 155 nm and fTi is 328.8 nm). The enlarged surface area by increased roughness could create broader territory for cell proliferation which support the relatively higher proliferation on the fTi [11]. In the literature, most of the research focused on osteoblast differentiation related to the LIPSS. In general, formed LIPSS structures have a hydrophilic behavior and cell proliferation is positively affected by hydrophilicity [76],[77]. There are few studies about LIPSS with hydrophobic behavior but their interaction with the osteoblast cells have not been investigated. Therefore, comparison to the studies in the literature would not lead to a helpful conclusion. Effect of surface pattern on cell morphology was observed using SEM and immunocytochemistry staining. Figure 3.8. shows that MC3T3-E1 cells were more elongated on the fTi surface. Cells on pTi surface were round shape. On the mTi surface, most of the cells were round but elongated cells across 2 intersections of hemicycle patterns were also observed in the Figure 3.8. c-II. Cells on mTi and fTi formed more filopodia protrusions compared to the cells on the pTi surface. In general, perpendicular cell elongation to the LIPSS pattern was observed on fTi surface. The length of filopodia protrusions are not uniform on mTi and fTi surfaces [78]. Random distribution of cells on pTi and TCPS were observed compared to the organized alignment of cells on mTi and fTi surfaces, shown in the Figure 3.9. Figure 3.9.D shows the actin cytoskeleton was aligned perpendicular to hemicycle pattern and intense amount of actin filaments were observed at the intersections. According to the SEM and immunocytochemistry staining results, clear effect of surface pattern on cell morphology and alignment were observed.

6. CONCLUSION

In conclusion, BSA adsorption, conformational changes, cell (L929 and MC3T3-E1) cytotoxicity and proliferation were investigated on pTi, mTi and fTi surfaces. Surface characterization investigated by means of wettability, roughness and topography. Water contact angle values increased by laser texturing, in the mTi and fTi groups. Roughness was highest in the fTi group. The highest adsorbed-BSA amount was observed on pTi surface. With the highest roughness and water contact angle values, fTi surface resulted in the least BSA adsorption amount. The denaturation of BSA upon adsorption was higher on mTi and fTi compared to pTi surface. Cytotoxicity and proliferation of cells were investigated by MTT and alamarBlue assays, respectively. Laser texturing of Ti samples was not resulted in a cytotoxic effect based on indirect MTT assay results while direct MTT assays resulted in cytotoxic effect of Ti samples. Proliferation rates of MC3T3-E1 cells on 1st, 4th and 7th days were concluded with similar increasing trend on all Ti groups. The fTi surface enhanced cell proliferation relatively more than the other groups. Effect of surface pattern on cell morphology was observed using SEM and immunocytochemistry staining. Cells on mTi and fTi surface are distributed more regularly with actin filaments following to the surface pattern. As a result of this thesis, surface nanomorphology significantly influences protein adsorption, protein conformation, cell proliferation and cell morphology but it might not be sufficiently enhanced viability.

6.1 Further Studies

Higher BSA-adsorption was observed on the hydrophilic pTi surface. Laser texturing resulted in higher denaturation of BSA which was observed in BSA-adsorbed mTi and fTi surfaces. By the aim of analyzing surface modification effect on protein adsorption behavior better, different proteins could be investigated with the same surface patterns. For the surface characterization, surface charge should be included to

the study since it is one of the main parameters affecting the protein adsorption. A quantitative method like Micro-BCA or Bradford assay would be used to investigate protein adsorption for better evaluation of obtained XPS results. The effect of the pattern on cell behavior and protein adsorption could be studied together. These additional studies may provide a clearer explanation of the relationship between protein adsorption, cell behavior and surface properties.

REFERENCES

1. Stich, T., F. Alagboso, T. Krenek, T. Kovarik, V. Alt, and D. Docheva, "Implant bone interface: Reviewing the impact of titanium surface modifications on osteogenic processes in vitro and in vivo," *Bioengineering & Translational Medicine*, Vol. 7, p. e10239, July 2021.

2. Akdoğan, E., H. Tolga Şirin, H. Öztatlı, B. Kılıçarslan, C. Bayram, and B. Garipcan, "Adsorption behavior of serum proteins on anodized titanium is driven by surface nanomorphology," *Biointerphases*, Vol. 18, p. 061001, Dec. 2023.

3. Kong, J., and S. Yu, "Fourier Transform Infrared Spectroscopic Analysis of Protein Secondary Structures," *Acta Biochimica et Biophysica Sinica*, Vol. 39, no. 8, pp. 549–559, 2007. _eprint: https://onlinelibrary.wiley.com/doi/pdf/10.1111/j.1745-7270.2007.00320.x.

4. Johns Hopkins Medicine, "Anatomy of the bone." https://www.hopkinsmedicine.org/health/wellness-and-prevention/anatomy-of-the-bone, 2024. Accessed: 2024-07-19.

5. World Health Organization, "Ageing and health." https://www.who.int/news-room/fact-sheets/detail/ageing-and-health, 2024. Accessed: 2024-07-21.

6. Mordor Intelligence, "Dental implants market - industry report." https://www.mordorintelligence.com/industry-reports/dental-implants-market, 2024. Accessed: 2024-07-20.

7. Global Market Insights, "Dental implants market - industry report." https://www.gminsights.com/industry-analysis/dental-implants-market, 2024. Accessed: 2024-07-20.

8. Albrektsson, T., P.-I. Branemark, H.-A. Hansson, and J. Lindström, "Osseointegrated Titanium Implants: Requirements for Ensuring a Long-Lasting, Direct Bone-to-Implant Anchorage in Man," *Acta Orthopaedica Scandinavica*, Vol. 52, pp. 155–170, Jan. 1981. Publisher: Taylor & Francis _eprint: https://doi.org/10.3109/17453678108991776.

9. Shah, F. A., P. Thomsen, and A. Palmquist, "Osseointegration and current interpretations of the bone-implant interface," *Acta Biomaterialia*, Vol. 84, pp. 1–15, Jan. 2019.

10. Yari, A., P. Fasih, S. Alborzi, H. Nikzad, and E. Romoozi, "Risk factors associated with early implant failure: A retrospective review," *Journal of Stomatology, Oral and Maxillofacial Surgery*, Vol. 125, p. 101749, Sept. 2024.

11. Chatzopoulos, G. S., and L. F. Wolff, "Dental implant failure and factors associated with treatment outcome: A retrospective study," *Journal of Stomatology, Oral and Maxillofacial Surgery*, Vol. 124, p. 101314, Apr. 2023.

12. Munakata, M., Y. Kataoka, K. Yamaguchi, and M. Sanda, "Risk Factors for Early Implant Failure and Selection of Bone Grafting Materials for Various Bone Augmentation Procedures: A Narrative Review," *Bioengineering*, Vol. 11, p. 192, Feb. 2024. Number: 2 Publisher: Multidisciplinary Digital Publishing Institute.

13. Barberi, J., and S. Spriano, "Titanium and protein adsorption: An overview of mechanisms and effects of surface features," *Materials*, Vol. 14, no. 7, 2021.

14. Lin, Z., and M. Hong, "Femtosecond Laser Precision Engineering: From Micron, Submicron, to Nanoscale," *Ultrafast Science*, Vol. 2021, Dec. 2021. Publisher: American Association for the Advancement of Science.

15. Sakallı, T. E., *THE EFFECT OF TITANIUM SURFACE TOPOGRAPHY ON BIOCOMPATIBILITY, HEMOCOMPATIBILITY, AND BACTERIAL BEHAVIOR*. Thesis, Boğaziçi University, 2022.

16. Akkan, C., D. Hür, L. Uzun, and B. Garipcan, "Amino acid conjugated self assembling molecules for enhancing surface wettability of fiber laser treated titanium surfaces," *Applied Surface Science*, Vol. 366, pp. 284–291, 2016.

17. SEER Training Modules, "Skeletal system: Bone tissue." https://training.seer.cancer.gov/anatomy/skeletal/tissue.html, 2024. Accessed: 2024-07-26.

18. Weiner, S., and W. Traub, "Bone structure: from angstroms to microns," *The FASEB Journal*, Vol. 6, no. 3, pp. 879–885, 1992. _eprint: https://onlinelibrary.wiley.com/doi/pdf/10.1096/fasebj.6.3.1740237.

19. Florencio Silva, R., G. R. D. S. Sasso, E. Sasso Cerri, M. J. Simoes, and P. S. Cerri, "Biology of Bone Tissue: Structure, Function, and Factors That Influence Bone Cells," *BioMed Research International*, Vol. 2015, pp. 1–17, 2015.

20. Sromova, V., D. Sobola, and P. Kaspar, "A Brief Review of Bone Cell Function and Importance," *Cells*, Vol. 12, p. 2576, Jan. 2023. Number: 21 Publisher: Multidisciplinary Digital Publishing Institute.

21. Bellido, T., L. I. Plotkin, and A. Bruzzaniti, "Chapter 3 - Bone Cells," in *Basic and Applied Bone Biology (Second Edition)* (Burr, D. B., and M. R. Allen, eds.), pp. 37–55, Academic Press, Jan. 2019.

22. Ansari, N., and N. Sims, *The Cells of Bone and Their Interactions*, Vol. 262. 01 2019.

23. Perez Castrillon, J. L., and J. A. Riancho del Moral, "Chapter 64 - Nutrients and Gene Expression Affecting Bone Metabolism," in *Principles of Nutrigenetics and Nutrigenomics* (Caterina, R. D., J. A. Martinez, and M. Kohlmeier, eds.), pp. 489–495, Academic Press, Jan. 2020.

24. Choi, J. U. A., A. W. Kijas, J. Lauko, and A. E. Rowan, "The Mechanosensory Role of Osteocytes and Implications for Bone Health and Disease States," *Frontiers in Cell and Developmental Biology*, Vol. 9, Feb. 2022. Publisher: Frontiers.

25. Williams, D., "The science and applications of biomaterials," *International Journal of Materials and Product Technology*, Vol. 10, pp. 360–377, Jan. 1995. Publisher: Inderscience Publishers.

26. Park, J. B., *Biomaterials Science and Engineering*, Springer Science & Business Media, Dec. 2012. Google-Books-ID: y9rTBwAAQBAJ.

27. Koons, G. L., M. Diba, and A. G. Mikos, "Materials design for bone-tissue engineering," *Nature Reviews Materials*, Vol. 5, pp. 584–603, Aug. 2020. Publisher: Nature Publishing Group.

28. Soman, S., and A. R. Ajitha, "18 - Life cycle assessment of metallic biomaterials," in *Fundamental Biomaterials: Metals* (Balakrishnan, P., S. M s, and S. Thomas, eds.), Woodhead Publishing Series in Biomaterials, pp. 411–423, Woodhead Publishing, Jan. 2018.

29. Migliaresi, C., "Chapter I.2.9 - Composites," in *Biomaterials Science (Third Edition)* (Ratner, B. D., A. S. Hoffman, F. J. Schoen, and J. E. Lemons, eds.), pp. 223–241, Academic Press, Jan. 2013.

30. Chen, Q., and G. A. Thouas, "Metallic implant biomaterials," *Materials Science and Engineering: R: Reports*, Vol. 87, pp. 1–57, Jan. 2015.

31. Geetha, M., A. K. Singh, R. Asokamani, and A. K. Gogia, "Ti based biomaterials, the ultimate choice for orthopaedic implants â A review," *Progress in Materials Science*, Vol. 54, pp. 397–425, May 2009.

32. Yaghoubi, S., C. Schwietert, and J. McCue, "Biological roles of titanium," *Biological Trace Element Research*, Vol. 78, no. 1-3, pp. 205–217, 2000.

33. Gasik, M., "Understanding biomaterial-tissue interface quality: combined in vitro evaluation," *Science and Technology of Advanced Materials*, Vol. 18, pp. 550–562, July 2017.

34. T., A., and J. C., "Osteoinduction, osteoconduction and osseointegration," *European spine journal : official publication of the European Spine Society, the European Spinal Deformity Society, and the European Section of the Cervical Spine Research Society*, Vol. 10 Suppl 2, pp. S96–101, 11 2001.

35. Garcia, A. J., "CHAPTER 36 - Surface Modification of Biomaterials," in *Principles of Regenerative Medicine (Second Edition)* (Atala, A., R. Lanza, J. A. Thomson, and R. Nerem, eds.), pp. 663–673, San Diego: Academic Press, Jan. 2011.

36. Amani, H., H. Arzaghi, M. Bayandori, A. S. Dezfuli, H. Pazoki-Toroudi, A. Shafiee, and L. Moradi, "Controlling Cell Behavior through the Design of Biomaterial Surfaces: A Focus on Surface Modification Techniques," *ADVANCED MATERIALS INTERFACES*, Vol. 6, p. 1900572, July 2019. Num Pages: 30 Place: Hoboken Publisher: Wiley Web of Science ID: WOS:000478635700012.

37. Kyriakides, T. R., "Chapter 5 - Molecular Events at Tissue -Biomaterial Interface," in *Host Response to Biomaterials* (Badylak, S. F., ed.), pp. 81–116, Oxford: Academic Press, Jan. 2015.

38. Fabre, H., D. Mercier, A. Galtayries, D. Portet, N. Delorme, and J.-F. Bardeau, "Impact of hydrophilic and hydrophobic functionalization of flat TiO2/Ti surfaces on proteins adsorption," *Applied Surface Science*, Vol. 432, pp. 15–21, Feb. 2018.

39. Gonçalves, S., F. Dourado, and L. R. Rodrigues, "Overview on Cell-Biomaterial Interactions," in *Advanced Polymers in Medicine* (Puoci, F., ed.), pp. 91–128, Cham: Springer International Publishing, 2015.

40. Saran, R., K. Ginjupalli, S. D. George, S. Chidangil, and V. K. Unnikrishnan, "LASER as a tool for surface modification of dental biomaterials: A review," *HELIYON*, Vol. 9, p. e17457, June 2023. Num Pages: 16 Place: Cambridge Publisher: Cell Press Web of Science ID: WOS:001042991900001.

41. Shivakoti, I., G. Kibria, R. Cep, B. B. Pradhan, and A. Sharma, "Laser Surface Texturing for Biomedical Applications: A Review," *Coatings*, Vol. 11, p. 124, Feb. 2021. Number: 2 Publisher: Multidisciplinary Digital Publishing Institute.

42. Przekora, A., "The summary of the most important cell-biomaterial interactions that need to be considered during in vitro biocompatibility testing of bone scaffolds for tissue engineering applications," *Materials Science and Engineering: C*, Vol. 97, pp. 1036–1051, Apr. 2019.

43. Yang, W.-E., and H.-H. Huang, "Multiform tio2 nano-network enhances biological response to titanium surface for dental implant applications," *Applied Surface Science*, Vol. 471, pp. 1041–1052, 2019.

44. Zanna, S., C. Compere, and P. Marcus, "XPS characterisation of BSA adsorption on stainless steel," in *Passivation of Metals and Semiconductors, and Properties of Thin Oxide Layers* (Marcus, P., and V. Maurice, eds.), pp. 365–370, Amsterdam: Elsevier Science, Jan. 2006.

45. Siow, K. S., L. Britcher, S. Kumar, and H. J. Griesser, "QCM-D and XPS study of protein adsorption on plasma polymers with sulfonate and phosphonate surface groups," *Colloids and Surfaces B: Biointerfaces*, Vol. 173, pp. 447–453, Jan. 2019.

46. AZoM, "Grade 2 Unalloyed Ti (âPureâ) 50A (UNS R50400)." https://www.azom.com/article.aspx?ArticleID=9413, 2024. Accessed: 2024-08-10.

47. Alpakut, G., M. B. Ünlü, and S. Yavas, "Femtosecond-pulsed glass welding of chemically tempered aluminosilicate glasses," in *Laser-based Micro- and Nanoprocessing XV*, Vol. 11674, pp. 229–235, SPIE, Mar. 2021.

48. Alpakut, G., I. Atespare, M. B. Ünlü, and S. Yavas, "High throughput fs-pulsed-glass welding via spiral scanning system," in *Laser-based Micro- and Nanoprocessing XV*, Vol. 11674, pp. 92–98, SPIE, Mar. 2021.

49. Akdoğan, E., "Protein adsorption on poly-3-hydroxybutyrate and poly(3-hydroxybutyrate-co-3-hydroxyvalerate): Adsorption isotherms and conformational analysis of the adsorbed protein," *Hacettepe Journal of Biology and Chemistry*, Vol. 50, 12 2021.

50. Karasu, T., F. Z. Erkoc-Biradli, M. Ö. Öztürk-Öncel, C. Armutcu, L. Uzun, B. Garipcan, and M. E. Çorman, "Synthesis and characterization of stimuli-responsive hydrogels: evaluation of external stimuli influence on L929 fibroblast viability," *Biomedical Physics & Engineering Express*, Vol. 8, p. 055004, July 2022. Publisher: IOP Publishing.

51. Öztürk-Öncel, M. Ö., F. Z. Erkoc-Biradli, R. Rasier, M. Marcali, C. Elbuken, and B. Garipcan, "Rose petal topography mimicked poly(dimethylsiloxane) substrates for enhanced corneal endothelial cell behavior," *Materials Science and Engineering: C*, Vol. 126, p. 112147, July 2021.

52. Garipcan, B., S. Maenz, T. Pham, U. Settmacher, K. Jandt, J. Zanow, and J. Bossert, "Image analysis of endothelial microstructure and endothelial cell dimensions of human arteries â a preliminary study," *Advanced Engineering Materials*, Vol. 13, pp. B54 – B57, 02 2011.

53. Erenay, B., "The effect of bone surface mimicked magnetic particle embedded pdms membranes on human osteoblast cell behavior," Master's thesis, Biomedical Engineering Institute.

54. Bonse, J., S. Kirner, and J. Krüger, "Laser-Induced Periodic Surface Structures (LIPSS)," in *Handbook of Laser Micro- and Nano-Engineering* (Sugioka, K., ed.), pp. 1–59, Cham: Springer International Publishing, 2020.

55. Mukherjee, S., S. Dhara, and P. Saha, "Enhancing the biocompatibility of Ti6Al4V implants by laser surface microtexturing: an in vitro study," *The International Journal of Advanced Manufacturing Technology*, Vol. 76, pp. 5–15, Jan. 2015.

56. Kuczynska-ZemÅa, D., P. Kwasniak, J. Marczak, J. Bonarski, J. Smolik, and G. Halina, "Laser surface treatment and the resultant hierarchical topography of ti grade 2 for biomedical application," *Applied Surface Science*, Vol. 390, 08 2016.

57. Akkan, C. K., "Rapid hierarchical structuring of titanium surface by modulated fiber laser: Protecting the native surface chemistry," *Materials Letters*, Vol. 183, pp. 26–29, Nov. 2016.

58. Klos, A., X. Sedao, T. E. Itina, C. Helfenstein-Didier, C. Donnet, S. Peyroche, L. Vico, A. Guignandon, and V. Dumas, "Ultrafast Laser Processing of Nanostructured Patterns for the Control of Cell Adhesion and Migration on Titanium Alloy," *Nanomaterials*, Vol. 10, p. 864, May 2020. Number: 5 Publisher: Multidisciplinary Digital Publishing Institute.

59. Zemaitis, A., A. Mimidis, A. Papadopoulos, P. Gecys, G. Raciukaitis, E. Stratakis, and M. Gedvilas, "Controlling the wettability of stainless steel from highly-hydrophilic to super-hydrophobic by femtosecond laser-induced ripples and nanospikes," *RSC Advances*, Vol. 10, p. 37956, 10 2020.

60. Kietzig, A.-M., S. G. Hatzikiriakos, and P. Englezos, "Patterned Superhydrophobic Metallic Surfaces," *Langmuir*, Vol. 25, pp. 4821–4827, Apr. 2009. Publisher: American Chemical Society.

61. Wenzel, R. N., "RESISTANCE OF SOLID SURFACES TO WETTING BY WATER," *Industrial & Engineering Chemistry*, Vol. 28, pp. 988–994, Aug. 1936. Publisher: American Chemical Society.

62. Yang, Y., S. Knust, S. Schwiderek, Q. Qin, Q. Yun, G. Grundmeier, and A. Keller, "Protein adsorption at nanorough titanium oxide surfaces: The importance of surface statistical parameters beyond surface roughness," *Nanomaterials*, Vol. 11, no. 2, 2021.

63. Alsaigh, R. A., "Enhancement of Surface Properties Using Ultrashort-Pulsed-Laser Texturing: A Review," *Crystals*, Vol. 14, p. 353, Apr. 2024. Number: 4 Publisher: Multidisciplinary Digital Publishing Institute.

64. Sarkar, S., and S. Kundu, "Protein (BSA) adsorption on hydrophilic and hydrophobic surfaces," *Materials Today: Proceedings*, May 2023.

65. Deligianni, D. D., N. Katsala, S. Ladas, D. Sotiropoulou, J. Amedee, and Y. F. Missirlis, "Effect of surface roughness of the titanium alloy Ti6Al4V on human bone marrow cell response and on protein adsorption," *Biomaterials*, Vol. 22, pp. 1241–1251, June 2001.

66. Keller, T. F., J. Reichert, T. P. Thanh, R. Adjiski, L. Spiess, L. Berzina-Cimdina, K. D. Jandt, and J. Bossert, "Facets of protein assembly on nanostructured titanium oxide surfaces," *Acta Biomaterialia*, Vol. 9, pp. 5810–5820, Mar. 2013.

67. Fologea, D., B. Ledden, D. S. McNabb, and J. Li, "Electrical characterization of protein molecules by a solid-state nanopore," *Applied physics letters*, Vol. 91, pp. 053901–1–053901–3, July 2007.

68. Stevie, F. A., and C. L. Donley, "Introduction to x-ray photoelectron spectroscopy," *Journal of Vacuum Science & Technology A: Vacuum, Surfaces, and Films*, Vol. 38, p. 063204, Dec. 2020.

69. Roach, P., D. Farrar, and C. C. Perry, "Interpretation of protein adsorption: surface-induced conformational changes," *Journal of the American Chemical Society*, Vol. 127, pp. 8168–8173, June 2005.

70. Roach, P., D. Farrar, and C. C. Perry, "Surface Tailoring for Controlled Protein Adsorption:â Effect of Topography at the Nanometer Scale and Chemistry," *Journal of the American Chemical Society*, Vol. 128, pp. 3939–3945, Mar. 2006. Publisher: American Chemical Society.

71. Sadat, A., and I. J. Joye, "Peak fitting applied to fourier transform infrared and raman spectroscopic analysis of proteins," *Applied Sciences*, 2020.

72. Barberi, J., L. Mandrile, L. Napione, A. M. Giovannozzi, A. M. Rossi, A. Vitale, S. Yamaguchi, and S. Spriano, "Albumin and fibronectin adsorption on treated titanium surfaces for osseointegration: An advanced investigation," *Applied Surface Science*, Vol. 599, p. 154023, Oct. 2022.

73. Wadajkar, A. S., C. Ahn, K. T. Nguyen, Q. Zhu, and T. Komabayashi, "In vitro cytotoxicity evaluation of four vital pulp therapy materials on l929 fibroblasts," *ISRN dentistry*, Vol. 2014, p. 191068, 2014.

74. Takamori, E. R., R. Cruz, F. GonÃ§alvez, R. V. Zanetti, A. Zanetti, and J. M. Granjeiro, "Effect of Roughness of Zirconia and Titanium on Fibroblast Adhesion," *Artificial Organs*, Vol. 32, no. 4, pp. 305–309, 2008. _eprint: https://onlinelibrary.wiley.com/doi/pdf/10.1111/j.1525-1594.2008.00547.x.

75. Chen, P., M. Miyake, M. Tsukamoto, Y. Tsutsumi, and T. Hanawa, "Response of pre-osteoblasts to titanium with periodic micro/nanometer scale grooves produced by femtosecond laser irradiation,"

76. Wu, Q.-X., T.-L. Chang, Z.-C. Chen, W.-T. Hsiao, and S.-P. Huang, "Investigation of ultrafast laser surface patterning and nanocrystalline formation on CrTiN alloy films for enhanced cell proliferation," *Applied Physics A*, Vol. 130, p. 161, Feb. 2024.

77. Raimbault, O., S. Benayoun, K. Anselme, C. Mauclair, T. Bourgade, A.-M. Kietzig, P.-L. Girard-Lauriault, S. Valette, and C. Donnet, "The effects of femtosecond laser-textured Ti-6Al-4V on wettability and cell response," *Materials Science and Engineering: C*, Vol. 69, pp. 311–320, Dec. 2016.

78. Lee, B. E. J., H. Exir, A. Weck, and K. Grandfield, "Characterization and evaluation of femtosecond laser-induced sub-micron periodic structures generated on titanium to improve osseointegration of implants," *Applied Surface Science*, Vol. 441, pp. 1034–1042, May 2018.